พอลิแอนิลีน/มอนต์มอริลโลไนต์นาโนคอมพอสิต สำหรับป้องกันการกัดกร่อนของเหล็กกล้า

นางสาวปัทมา ภิรมย์รื่น

วิทยานิพนธ์นี้เป็นส่วนหนึ่งของการศึกษาตามหลักสูตรปริญญาวิทยาศาสตรมหาบัณฑิต
สาขาวิชาปิโตรเคมีและวิทยาศาสตร์พอลิเมอร์
คณะวิทยาศาสตร์ จุฬาลงกรณ์มหาวิทยาลัย
ปีการศึกษา 2555

POLYANILINE/MONTMORILLONITE NANOCOMPOSITES FOR CORROSION PROTECTION OF STEEL

Miss Pattama Piromruen

A Thesis Submitted in Partial Fulfillment of the Requirements
for the Degree of Master of Science Program in Petrochemistry and Polymer Science
Faculty of Science
Chulalongkorn University
Academic Year 2012

Thesis Title	POLYANILINE/MONTMORILLONITE NANOCOMPOSITES FOR CORROSION PROTECTION OF STEEL
By	Miss Pattama Piromruen
Field of Study	Petrochemistry and Polymer Science
Thesis Advisor	Professor Pattarapan Prasassarakich, Ph.D.
Thesis Co-advisor	Suwadee Kongparakul, Ph.D.

Accepted by the Faculty of Science, Chulalongkorn University in Partial Fulfillment of the Requirements for the Master's Degree

..…….. Dean of the Faculty of Science
(Professor Supot Hannongbua, Dr.rer.nat.)

THESIS COMMITTEE

…….. Chairman
(Associate Professor Tharapong Vitidsant, Ph.D.)

…….……. Thesis Advisor
(Professor Pattarapan Prasassarakich, Ph.D.)

…….……. Thesis Co-advisor
(Suwadee Kongparakul, Ph.D.)

…….. Examiner
(Assistant Professor Varawut Tangpasuthadol, Ph.D.)

…….. External Examiner
(Associate Professor Ittipol Jangchud, Ph.D.)

ปัทมา ภิรมย์รื่น: พอลิแอนิลีน/มอนต์มอริลโลไนต์นาโนคอมพอสิตสำหรับป้องกันการกัดกร่อนของเหล็กกล้า. (POLYANILINE/MONTMORILLONITE NANO-COMPOSITES FOR CORROSION PROTECTION OF STEEL) อ.ที่ปรึกษาวิทยานิพนธ์หลัก: ศ.ดร.ภัทรพรรณ ประศาสน์สารกิจ, อ.ที่ปรึกษาวิทยานิพนธ์ร่วม: อ.ดร. สุวดี ก้องพารากุล, 74 หน้า.

งานวิจัยนี้เป็นการศึกษาการสังเคราะห์นาโนคอมพอสิตของพอลิแอนิลีนและมอนต์มอริล-โลไนต์ (PANI/MMT) สำหรับป้องกันการกัดกร่อนของเหล็กกล้า ด้วยวิธีพอลิเมอไรเซชันแบบออกซิเดชันทางเคมีแบบอินซิทู พอลิเมอร์นาโนคอมพอสิตถูกเตรียมขึ้นโดยใช้ปริมาณมอนต์มอริล-โลไนต์ ร้อยละ 1, 3, 5 และ 7 โดยน้ำหนักเทียบกับน้ำหนักมอนอเมอร์ พบว่ามีค่าการเปลี่ยนแปลงมอนอเมอร์สูงสุดที่ร้อยละ 75.8 เมื่อเติมมอนต์มอริลโลไนต์ร้อยละ 1 โดยน้ำหนัก จากการศึกษาองค์ประกอบของพอลิแอนิลีนและนาโนคอมพอสิตด้วยเครื่องฟูเรียทรานฟอร์มอินฟราเรดสเปค - โตรสโคปี พบว่า PANI/MMT นาโนคอมพอสิตประกอบด้วยหมู่ฟังก์ชันไฮดรอกซิล (-OH) ไซยาไนด์ (-CN) และเอไมด์ (RCONHR) ซึ่งสอดคล้องกับคุณลักษณะเฉพาะของพอลิแอนิลีนและมอนต์มอริลโลไนต์ จากการพิสูจน์เอกลักษณ์ด้วยเครื่องเอ็กซเรย์ดิฟแฟรคโตมิเตอร์ พบหลักฐานว่าอนุภาคพอลิแอนิลีนแทรกสอดระหว่างชั้นของมอนต์มอริลโลไนต์ จากการศึกษาสัณฐานวิทยาของ PANI/MMT นาโนคอมพอสิตโดยใช้กล้องจุลทรรศน์อิเล็กตรอนแบบส่องกราด พบว่านาโนคอมพอสิตประกอบด้วยพอลิแอนิลีนที่มีลักษณะเป็นทรงกลมกระจายตัวแทรกอยู่ในชั้นของมอนต์มอริลโลไนต์ จากการศึกษาสมบัติเชิงความร้อน พบว่านาโนคอมพอสิตมีเสถียรภาพเชิงความร้อนที่สูงขึ้นเมื่อเพิ่มปริมาณมอนต์มอริลโลไนต์ จากการศึกษาการกัดกร่อน พบว่าเหล็กกล้าที่เคลือบด้วย PANI/MMT นาโนคอมพอสิต สามารถป้องกันการกัดกร่อนในสารละลายกรดซัลฟิวริก ความเข้มข้น 1.0โมลาร์ได้ดีกว่าเหล็กกล้าที่เคลือบด้วย PANI การเพิ่มปริมาณมอนต์มอริลโลไนต์ในนาโนคอมพอสิตและความหนาของฟิล์มสามารถเพิ่มคุณสมบัติของการป้องกันการกัดกร่อนได้ดี เนื่องจากช่วยลดการซึมผ่านของสารกัดกร่อนมายังผิวของเหล็กกล้า โดยที่เหล็กกล้าที่เคลือบด้วย PANI/MMT นาโนคอมพอสิตที่มีปริมาณมอนต์มอริลโลไนต์ร้อยละ 5 โดยน้ำหนักเทียบกับน้ำหนักมอนอเมอร์และมีความหนาของฟิล์ม 50 ไมโครเมตร สามารถป้องกันการกัดกร่อนของเหล็กกล้าได้ดีที่สุด

สาขาวิชา ปิโตรเคมีและวิทยาศาสตร์พอลิเมอร์ ลายมือชื่อนิสิต……..……

ปีการศึกษา 2555 ลายมือชื่อ อ.ที่ปรึกษาวิทยานิพนธ์หลัก…..……....

ลายมือชื่อ อ.ที่ปรึกษาวิทยานิพนธ์ร่วม…..……....

5372283823: MAJOR PETROCHEMISTRY AND POLYMER SCIENCE
KEYWORDS: POLYANILINE/ MONTMORILLONITE/ NANOCOMPOSITES

PATTAMA PIROMRUEN: POLYANILINE/MONTMORILLONITE NANOCOMPOSITES FOR CORROSION PROTECTION OF STEEL. ADVISOR: PROF. PATTARAPAN PRASASSARAKICH, Ph.D., CO-ADVISOR: SUWADEE KONGPARAKUL, Ph.D., 74 pp.

Polyaniline/montmorillonite (PANI/MMT) nanocomposites were synthesized by *in situ* chemical oxidative polymerization for corrosion protection of steel. The polymer clay nanocomposites were prepared by varying the MMT content (1, 3, 5 and 7 wt% based on monomer content). The results showed that the maximum monomer conversion was 75.8% at MMT content of 1 wt%. PANI/MMT nanocomposites was characterized by Fourier-transform infrared spectroscopy (FT-IR). The results showed functional groups of hydroxyl (-OH), cyanide (-CN) and amide (RCONHR) which attributed to PANI and MMT characteristic. PANI intercalated between the layers of MMT was confirmed by X-ray diffractometer. The montmorillonite layer and the agglomerated spheres of polyaniline dispersed in the nanocomposites morphology were observed by scanning electron microscope (SEM). The thermal stability of PANI/MMT nanocomposites, examined by thermogravimetric analysis (TGA), was enhanced by an increasing in MMT content. From corrosion study in 1.0 M sulfuric acid solution, steel coated with PANI/MMT nanocomposites film showed better corrosion resistant than steel coated with PANI film. The increased in the amount of MMT in nanocomposites and film thickness could improve anticorrosive properties due to an increasing in tortuosity of diffusion pathway of corrosion agents. The steel coated with 50 μm thickness of PANI/MMT (5 wt%) showed the best corrosion resistance comparing to the other coated steel.

Field of Study:Petrochemistry and Polymer Science Student's Signature……

Academic Year: 2012 Advisor's Signature……...

Co-advisor's Signature…….

ACKNOWLEDGEMENTS

The author would like to express her gratitude to her supervisors, Prof. Dr. Pattarapan Prasassarakich and co-advisor, Dr.Suwadee Kongparakul (Department of Chemistry, Faculty of Science and Technology, Thammasat University) for her encouraging guidance, supervision and helpful suggestion throughout her research. The author also would like to acknowledge Assoc. Prof. Dr. Tharapong Vitidsant, Assist. Prof. Dr. Varawut Tangpasuthadol, and Assoc. Prof. Dr. Ittipol Jangchud for their participation on the dissertation chairman and members of thesis committee, respectively.

The author would like to gratefully acknowledge to Asst. Prof. Dr. Nisit Tantavichet for his helpful suggestion throughout her research, Southern Clay Product Co., Ltd. for the support of the montmorillonite clay for this research, Program of Petrochemistry and Polymer Science, Department of Chemical Technology, Faculty of Science, Chulalongkorn University.

A warm thank is expressed to all of her friends in the laboratory for their friendships and help during the course of her graduate research.

Finally, and most of all, the author would like to express her deep appreciate to her family for their love, support and endless encouragement throughout her entire study.

CONTENTS

Page

Page

Page

LIST OF TABLES

LIST OF FIGURES

Figure **Page**

Figure **Page**

Figure **Page**

LIST OF ABBREVIATIONS

APS	:	Ammonium persulfate
CR	:	Corrosion rate
E_{corr}	:	Corrosion potential
FTIR	:	Fourier Transform Infrared spectroscopy
I_{corr}	:	Corrosion current
MMT	:	Montmorillonite clay (Cloisite15A)
NMP	:	1-Methyl-2-pyrrolidone
PANI	:	Polyaniline
SEM	:	Scanning Electron Microscopy
TGA	:	Thermogravimatric Analysis
XRD	:	X-Ray Diffraction

CHAPTER I

INTRODUCTION

1.1 The Purpose of the Investigation

Corrosion can lead to failures in plant infrastructure and machines which are usually expensive to repair, expensive in terms of lost or contaminated products, environmental damage, and human safety. Decisions regarding the future integrity of a structure or its components depend upon an accurate estimation of the conditions affecting its corrosion and rate of deterioration [1]. Therefore, the efforts to develop more efficient and environmentally compliant methods to prevent corrosion have been ongoing throughout this century. Approaches commonly used to reduce the rate of corrosion are protective coatings, cathodic protection, addition of inhibitors and very pure metals, as shown in Figure 2.1.

Conducting polymers have become one of the most attractive subjects of investigation. Their unique properties including electrical conductivity, electrochemical properties and mechanical strength make these polymers useful in many applications such as electrochemical sensor, rechargeable batteries and corrosion protection [2]. Polyaniline (PANI) is one of the most important conducting polymers due to its high electrical conductivity, electrochemical properties, environmental stability, facile synthesis and low cost [3]. However, there are some major drawbacks, such as poor mechanical performance and least anticorrosive properties, which limit its applications. These problems can be solved by addition of filler leading to the synthesis of polymer-clay nanocomposites (PCN). Therefore, the addition of montmorillonite clay into PANI could improve the mechanical strength, thermal stability, fire retardant, gas barrier and anticorrosive properties [9-10]. The modified montmorillonite clay with organic compounds could be compatible with polymers and a good dispersion was obtained because of the nanosize of clay. PCN can be synthesized by various methods, such as *in situ* interactive polymerization and solution or melts or emulsion intercalation method. *In situ* interactive polymerization is a suitable method for conducting polymer synthesis due to the fact that this method

can be initiated either by heat or radiation, by the diffusion of a suitable initiator, or by an organic initiator or catalyst fixed through cation exchange inside the interlayer before the swelling step [4].

In the research work, polyaniline/montmorillonite (PANI/MMT) nanocomposites were synthesized by *in situ* chemical oxidative polymerization. The anticorrosive properties of polyaniline/montmorillonite (PANI/MMT) nanocomposites on steel were investigated.

1.2 The Objective

The objectives of thesis can be summarized as follows:

1. To prepare the polyaniline and PANI/MMT nanocomposites by *in situ* chemical oxidation polymerization.
2. To investigate the effects of montmorillonite loading on the monomer conversion and thickness layer of PANI/MMT nanocomposites.
3. To study the thermal properties, morphology and corrosion prevention studies of PANI/MMT nanocomposites.

1.3 Scope of the Investigation

The experimental procedure for this research was presented as follows:

1. Literature survey and in-depth study for this research work.
2. Prepare the polyaniline and PANI/MMT nanocomposites by *in situ* chemical oxidation polymerization and study the effects of montmorillonite loading at 1, 3, 5 and 7 wt% based on monomer.
3. Investigate the monomer conversion for preparation of polyaniline and PANI/MMT nanocomposites.
4. Characterize the polyaniline and PANI/MMT nanocomposites by Fourier transform infrared and X-ray diffraction.
5. Investigate the thermal properties and morphology of polyaniline and PANI/MMT nanocomposites.

6. Investigate thickness layer and corrosion protection of polyaniline and PANI/MMT nanocomposites.
7. Analyze data and summarize the results.

CHAPTER II

THEORY AND LITERATURE REVIEW

2.1 Polyaniline [5]

Polyaniline (PANI) is a conducting polymer. Polyaniline contains conjugated double bonds which can act as electronically conducting material which is conveniently doped by coupling with charge-transfer agents. Polyaniline consists of aniline repeating units to form a backbone of alternating nitrogen atoms and benzene rings.

Reduced repeating units Oxidized repeating units

Figure 2.1 General chemical structure of polyaniline [6]

Polyaniline exists in a variety of forms that differ in chemical and physical properties [14]. It can be classified into four groups depending upon the degree of oxidation of the nitrogen atoms including the leucoemeraldine base (PANI-LEB), emeraldine base (PANI-EB), pernigraniline base (PANI-PNB) and emeraldine salt (PANI-ES) as presented in Table 2.1. Polyaniline is a specific conducting polymer because of its conducting mechanism induced either by the oxidation of the polyleucoemeraldine base or by the protonation of the polyemeraldine base as shown in Figure 2.2(a).

Polyaniline is a typical phenylene-base polymer having a chemically flexible –NH– group in a polymer chain flanked either side by phenylene ring. The protonation, deprotonation and several other physico-chemical properties of polyaniline could be carried on due to the presence of the –NH– group. Conductivity of polymeraldine base is around 10 S/cm. Polyaniline is found to be the most useful because of good conductivity, environmental stability, ease of preparation and low cost [7]. The

mechanism of corrosion protection of PANI coated steel due to the formation of passivating iron oxide (Fe_2O_3 and Fe_3O_4), a redox reaction occurs between Fe and $(PANI)_{ox}$ (PANI oxidized state or PANI emeraldine salt (ES)) leading to $(PANI)_{red}$ (PANI neutral state and or PANI leuco base) to Fe^{2+}. In the presence of O_2 and H_2O it is assumed that the neutral from of PANI is reoxidized to $(PANI)_{ox}$, or PANI emeraldine salt (ES), while Fe^{2+} is oxidized to Fe^{3+} and transformed into Fe_2O_3 in the presence of OH^- resulting from the reduction of $O_2 + H_2O$ as shown in Figure 2.2(b) [34].

Table 2.1 The different forms of polyaniline [9].

Form	Name	Color	Conductivity($S.cm^{-1}$)
Reduced form	Leucuemeraldine base (PANI-LEB)	Yellow, White/clear	$< 10^{-5}$
Half oxidized form	Emeraldine base (PANI-EB)	Blue	$< 10^{-5}$
Oxidized form	Pernigraniline (PANI-PNB)	Blue/Violet	$< 10^{-5}$
	Emeraldine salt (PANI-ES)	Green	~15

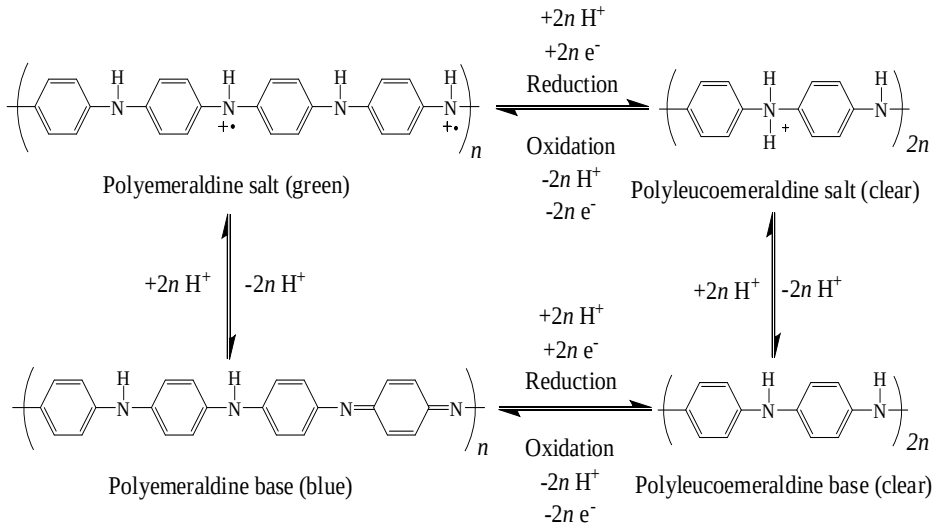

Figure 2.2 (a) Doping mechanisms of PANI [8]

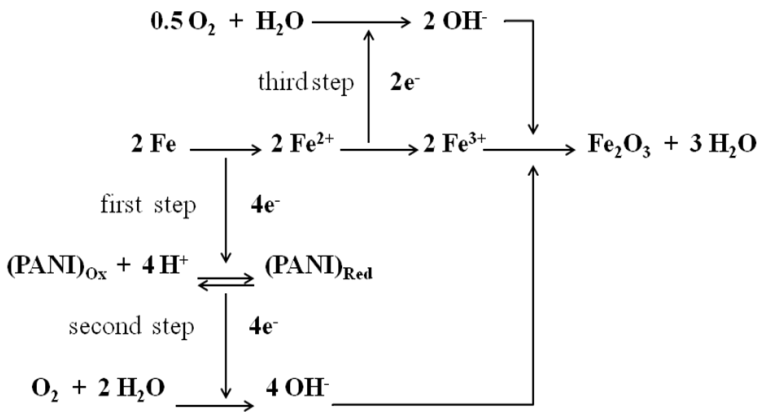

Figure 2.2 (b) Corrosion protection mechanism [34]

2.1.1 Synthesis of Polyaniline [9]

Polyaniline can be prepared by either chemical or electrochemical oxidation of aniline under acidic conditions. The synthesis of polymer by chemical or electrochemical methods depends upon the intended application of the polymer.

Chemical polymerization

The most common synthesis method of polyaniline is oxidative polymerization. The most preferred method for synthesis is to use hydrochloric or sulfuric acid with ammonium persulfate (APS) as an oxidant. However, the most popular synthesis pathway is under 1M aqueous hydrochloric acid solution. Oxidative polymerization is a two-electron change reaction and hence, the persulfate requirement is one mole per mole of a monomer. However, the smaller quantity of oxidant is used to avoid oxidative degradation of the polymer form. The obtained precipitate is polyemeraldine salt (PANI-ES), green colored.

Electrochemical polymerization

For electrochemical synthesis, several methods can be used galvanostatic, potentiostatic which a constant current is applied, cyclic voltammetry and other potentiodynamic methods which current and potential are varied with time. For all these techniques compose of a working electrode which the polymer is deposited, a

counter electrode (platinum grid) and a reference electrode (a saturated calomel electrode, SCE).

The different synthesis methods are also proposed including photochemical initialed polymerization, enzyme-catalyzed polymerization employing electron acceptors.

2.1.2 The Reaction Mechanism of Polyaniline [9]

The reaction mechanism of aniline polymerization is shown in Figure 2.3. First step is the aniline monomer from anilinium ion in acidic medium and chemical polymerization result in the formation of protonated, partially oxidized form of polyaniline. This step involves aniline forming radical cation. The second step is the coupling of –N in amine functional group and para-radical cation with consecutive re-aromatization of the di-cation. The final step is the oxidation process of the di-radical di-cation makes the fully oxidized pernigraniline salt form of polyaniline due to the high oxidizing power of oxidant; the oxidant used in the experiment was APS. This would create head to tail coupling is predominate some coupling in the ortho-position also occurs, obtained a conjugation defect in the final product.

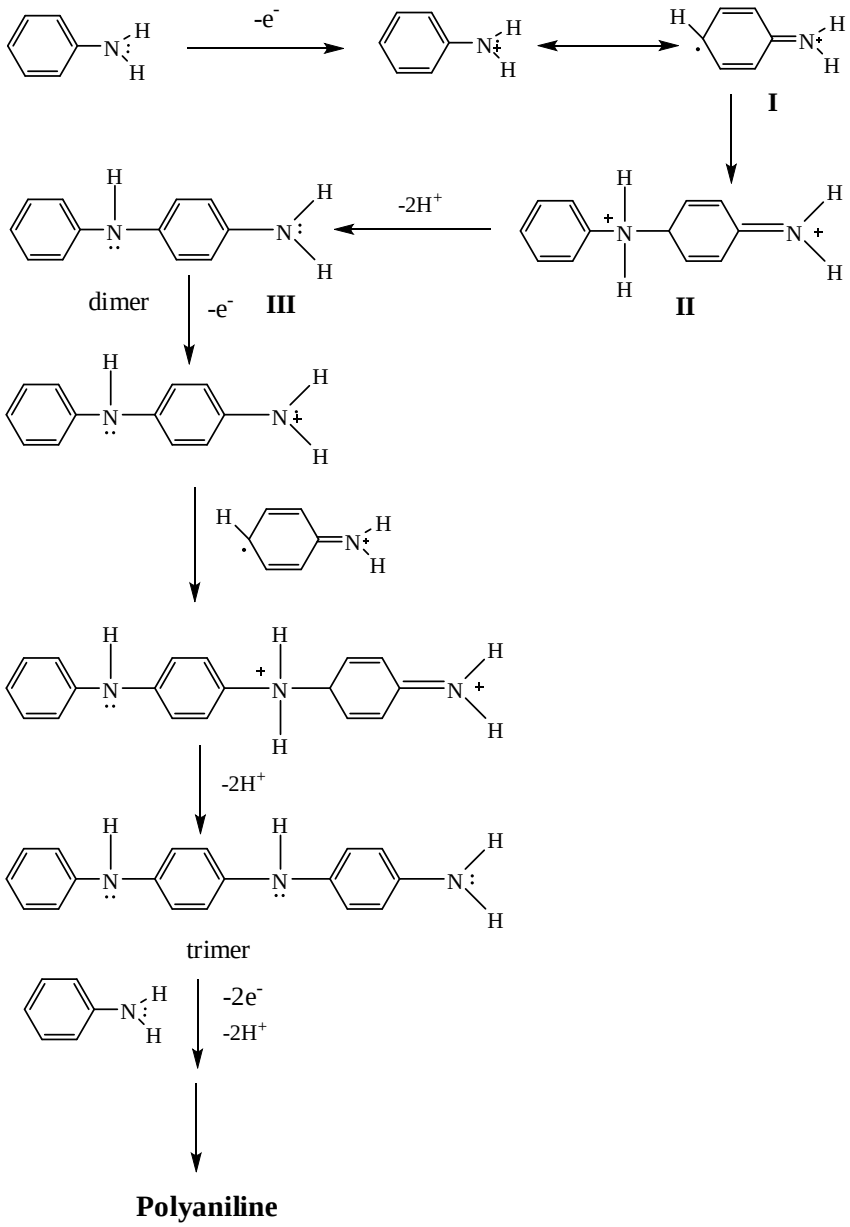

Figure 2.3 Reaction mechanism of aniline polymerization [9]

2.2 Clay [10]

Natural clay contains pure clay, mineral clay and non-clay mineral. The impurities including calcite, quartz, feldspars, iron oxides and humic acids are the most common components in the pure clay mineral. Calcite, iron oxides and humic acids can be eliminated by chemical treatments. Quartz and feldspars can be eliminated by sedimentation. However, traces of quartz are often found in the purified samples.

Types of clay can be classified by mainly chemical composition of clay mineral. Clay minerals are hydrous silicates which contain silica tetrahedral sheets and alumina octahedral sheets. There are four groups, including kaolinites, illites, smectites and vermiculites which difference in chemical structures and compositions.

The clay mineral can be identified by layer type and position of cation which substitute in alumina octahedral sheets as shown in Table 2.2.

Table 2.2 Type of clay minerals [10].

Characters	Kaolinites	Illites	Smectites	Vermiculites
Structure Type	1:1	2:1	2:1	2:1
Octahedral component	di-octahedral	Mostly di-octahedral	di- or tri-octahedral	Mostly tri-octahedral
Principal interlayer cations	Nil	K	Ca, Na	Mg
Interlayer water	Only in halloysite (one layer)	Some in hydromuscovite	Ca two layers; Na one layer	Two layer
Basal Spacing	7.1Å (10Å in halloysite)	10Å	Variable, moat ~15Å(for Ca)	Variable, 14.4Å when fully hydrated
Glycol	Taken up by halloysite only	No effect	Takes two layers glycol, 17Å	Takes one layers glycol, 14Å
Chemical formula	$Al_4Si_4O_{10}(OH)_8$	$K_{1.0\text{-}1.5}Al_4(Si,Al)_8O_{20}(OH)_4$	$M^+_{0.7}(Y^{3+},Y^{2+})_{4\text{-}6}(Si,Al)_8O_{20}(OH)_4 nH_2O$	$M^{2+}_{0.66}(Y^{2+},Y^{3+})_6(Si,Al)_8O_{20}(OH)_4 8H_2O$
Paragenesis	Alterlation of acid rocks, feldspars, etc. Acidic condition	Alterlation of micas, feldspars, etc. Akaline condition	Alterlation of basic rocks, or volcanic material. Akaline condition	Alterlation of biotite flakes or volcanic material, chlorites, hornblende, etc.

- Kaolinites group is 1:1 type of layer silicate and clay minerals in this group are kaolinite, dickite, nacrite and halloysite
- Illites group is 2:1 type of layer silicate which has potassium ion compensate charge in interlayer, including illite, hydrous mica, phengite, brammalite, glauconite and celadonite
- Smectites group is 2:1 type of layer silicate, including montmorillonite, beidellite, nontronite, hectrorite, saponite and sauconite
- Vermiculites group is 2:1 type of layer silicate which has magnesium ion compensate charge in interlayer

Smectite clay [10]

Smectite group can be expanded and attracted crystal structure when immerse in water or some organic solvent. The clay minerals in this group are beidellite, hectrorite, montmorillonite, nontronite, saponite and sauconite with different in chemical composition.

Smectite is a 2:1 type layered clay mineral which consists of two silica tetrahedral sheets coordinated silicon atoms fused and edge-shared alumina octahedral sheet of either alumina or magnesium hydroxide as shown in Figure 2.4. The distance between the plane in one layer and the corresponding plane in the next layer is called the basal spacing or *d*-spacing stacking of the layers leads to a regular Van der Waals gap between the layers called the interlayer or gallery. Isomorphic substitution within the layers generates negative charges that are counterbalanced by alkali and alkaline earth cations situated inside the galleries.

The layered silicate is swollen within the hydration and cation exchange. Interlayer surface and cation exchange inside the interlayer between smectite structure units is a unique property of smectite clays. The crystal structure of smectite clay can be detected by X-ray diffraction. The layer thickness is around 1 nm and lateral dimensions of these layers may differ 300 Å to several microns, giving an aspect ratio (length/thickness) greater than 1000 [11].

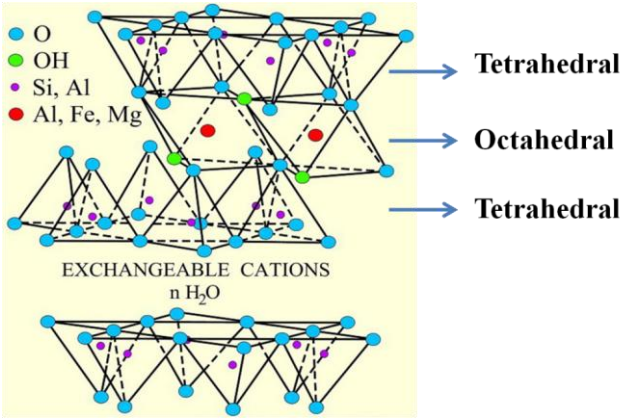

Figure 2.4 Illustration of T:O:T structure of montmorillonite clay [4]

Montmorillonite (MMT)

Montmorillonite (MMT) is the most commonly used layered silicates for the preparation of nanocomposites. The crystal lattice consists of layers where a central octahedral sheet of alumina or magnesium is fused to two external silica tetrahedral sheet. Montmorillonite has a potentially high surface area, low thermal expansion coefficient and high gas barrier property. According to the forces that hold the stacks together are relatively weak, the intercalation of small molecules between the layers is easy. The total amount of cations adsorbed in the clay interlayer, expressed in miliequivalents per hundred grams of dry clay, is called the cation exchange capacity (CEC). The high CEC was obtained by using sodium montmorillonite, as compared to the other clay minerals [25].

2.3 Polymer-Clay Nanocomposites [4, 5]

Polymer-clay nanocomposites (PCN) materials are formed through the union of two different materials which are organic polymer matrix and inorganic clay in nanoscale filler. The most popular used nanoscaled filler is based on the smectite class of aluminum silica clays, of which the most common representative is montmorillonite (MMT). The PCN show conspicuously enhanced mechanical, thermal and barrier properties compared to pure polymer.

2.3.1 Polymer-Clay Nanocomposites Preparation [5]

Polymer-clay nanocomposites or rubber-clay nanocomposites (RCN) have potential for many industries and academic researchers. PCN exhibit the remarkable properties at low filler loading compared with unfilled rubber compounds or conventional filled composites. The rubber-clay nanocomposites have been studied mainly on four well-known rubbery materials, natural rubber (NR), ethylene propylene diene rubber (EPDM), styrene-butadiene rubber (SBR), and nitrile rubber (NBR). However, some other types of elastomers such as silicon rubber, polybutadiene rubber, and ethylene propylene rubber also exist.

The preparative methods are divided into three main groups according to the processing techniques:

- melt intercalation
- intercalation of polymer
- *in situ* polymerization

Melt intercalation

This method has great advantage for the industrial process because of an environmental friendly process due to the absence of organic solvent. Polymer and layered silicate mixture are blended in the molten state under shear. The polymer chains diffuse from the molten polymer into the layered silicate galleries to form intercalated or delaminated nanocomposites.

Intercalation of polymer

This is based on a solvent system in which the polymer is soluble and the silicate layers are swollen. The layered silicate is first swollen and comes apart in the solvent. The monomer is dissolved in solvent and added to the solution when the solutions are mixed; the polymer chains intercalate and replace the solvent within the interlayer of the silicate. Upon solvent removal, the intercalated structure remains, resulting in polymer-clay nanocomposites.

Direct melt intercalation method

This is the simple method that has many advantages for the industrial process and mild environmental effect, due to the absence of solvents. In this method, rubber and modified layered silicate mixture are blended in the molten state under high shear. The rubber chains were melted into the silicate galleries to form intercalated or delaminated nanocomposites.

In situ polymerization

In this method, the layered silicate is swollen within the monomer solution or liquid monomer, so the polymer formation can occur between the intercalated sheets. Polymerization can be initiated either by radiation or heat, diffusion of a suitable

initiator and the additions of organic initiator or catalyst by fixed through cation exchange inside the interlayer before the swelling step.

2.3.2 Polymer-Clay Nanocomposites Structure [4]

A few weight percent of layered silicates are properly dispersed in the polymer matrix results in higher surface area for polymer-clay interaction as compared to conventional composites. Depending on the strength of interfacial interactions between the polymer matrix and layered silicate, three different types of polymer-clay nanocomposites can be produced as shown in Figure 2.5.

- Phase separated microcomposites or conventional composites: the polymer is unable to intercalate between the silicate sheets and the clay agglomerate is formed.

- Intercalated nanocomposites: the insertion of a polymer chain into the layered silicate structure occurs in a crystallographically regular fashion, regardless of the clay to polymer ratio. Intercalated nanocomposites are normally interlayer by a few molecular layers of polymer.

- Exfoliated nanocomposites: the individual clay layers are separated in a continuous polymer matrix by an average distances that depends on clay loading. Usually, the clay content of exfoliated nanocomposites is much lower than that of a intercalated nanocomposites.

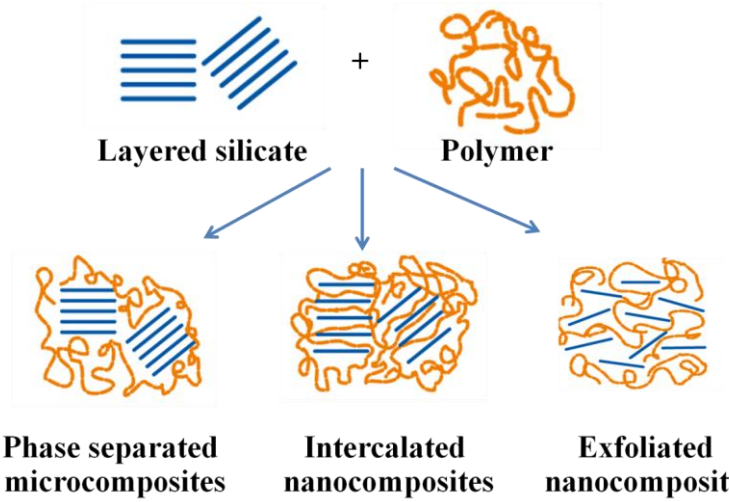

Figure 2.5 Possibility of polymer/layered silicate structure [12]

2.3.3 Characterization of Polymer-Clay Nanocomposites [5]

There are mainly two methods to characterize the structure of PCN. The most is X-ray diffraction (XRD) to determine the spacing between the clay layers. The sample preparation is relatively easy and the X-ray analysis can be performed within a few hours. However, one needs to be very careful with the interpretation of the results. Lack of sensitivity of the analysis and limits of the equipment can lead to wrong conclusions about the nanocomposites structure. Therefore, transmission electron microscopy (TEM) is a necessary complement to XRD. TEM gives a direct measurement of the special distribution of the layers but requires significant skills in specimen preparation and analysis.

X-Ray Diffraction

XRD is used to identify intercalated structures. In such nanocomposites, the repetitive multilayer structure is well preserved, allowing the interlayer spacing to be determined. The intercalation of the polymer chains usually increased the interlayer spacing, as compared with the spacing of the organoclay used, leading to a shift of the diffraction peak towards lower angle values. Angle and layer spacing values are being related to the Bragg's relation:

$$\lambda = 2d \sin\theta \tag{2.1}$$

where λ corresponds to the wave length of the X-ray radiation used in the diffraction experiment, d is the spacing between diffraction lattice planes and θ is the measured diffraction angle or glancing angle.

When exfoliated structure is concerned, no more diffraction peaks are visible in the XRD diffractograms due to large spacing between the layers (i.e. exceeding 8 nm in the case of ordered exfoliated structure) and loss of structure.

Transmission Electron Spectroscopy

Transmission Electron Spectroscopy (TEM) is used to characterize the nanocomposites morphology. Besides these two well-defined structures, other

intermediate organizations can exist presenting both intercalation and exfoliation was observed by TEM.

2.4 Corrosion [13]

Corrosion is a complex form of materials deterioration. Corrosion has been defined in many ways: (1) destruction of metal by chemical or electrochemical reaction with its environment, (2) destruction of materials by means other than straight mechanical and (3) extractive metallurgy in reverse. For example, one phase of extractive metallurgy is concerned with the production of iron and steel from iron ores (oxide), but steel may revert to oxide when rusting or corrosion occurs. Most environments are corrosive to a greater or lesser degree. Examples are air and moisture; fresh, distilled, or salt water; rural, urban and industrial atmospheres; steam and other gases such as chlorine, ammonia, hydrogen sulfide, sulfur dioxide, and fuel gases; mineral acids such as hydrochloric, sulfuric and nitric; organic acids such as naphthenic, acetic, and formic; alkalis; soils; solvents such as alcohols and dry cleaning fluids; vegetable and petroleum oils; and a variety of food products. Corrosion of steel and iron by air and moisture is very common and results in a tremendous annual loss. The rapid rusting of clean unprotected iron and steel is well known to practically everyone. The recent trend in the chemical process industries toward higher temperatures and pressures has made possible new processes or improvements in old processes. For example, better yields, greater speed, or lower cost of production are now possible. Higher temperatures and pressures unfortunately also involve more severe corrosion.

This is the accepted theory and it is actually quite simple. There are two basic requirements: (1) anodes and cathodes must be present to form a cell, and (2) direct current must flow. The anodes and cathodes may be very close together (local cell) or they may be far apart. The current may be self-induced or it may be impressed on the system from an outside source. The anode is the area where corrosion occurs and where current leaves the metal and enters the solution. The cathode is the area where no corrosion occurs and where current enters the metal from the solution. Anodes and cathodes can form on a single piece of metal because of local differences in the metal

or in the environment. The metal at the anode dissolves and becomes an ion. It is oxidized and loses electrons. For example, iron dissolves and loses two electrons to become the ferrous ion Fe^{2+}. The iron atom detaches itself and goes into solution as a ferrous ion. The electrons are left on the metal and travel through it to the cathode area. These electrons are accepted at the cathode area.

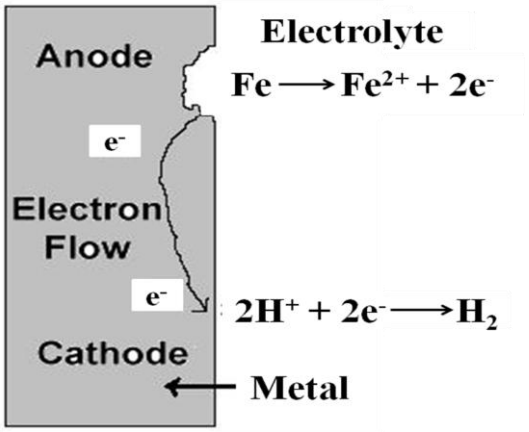

Figure 2.6 Basic diagram showing requirements for corrosion of metals [13]

Immersion in an electrolyte or conducting fluid is required to complete the circuit or to carry the current from the anode or anodic area to the cathode or cathodic area. For example, high (purity)-resistance water is used in certain applications to keep corrosion at a very low rate. However, most waters such as tap water and seawater are not pure and are good conductors. Figure 2.6 illustrates the ionization of water ($H_2O = H^+ + OH^-$).

Corrosion of iron in pure water (and acids) occurs as follows (e^- represents an electron):

$$Fe = Fe^{2+} + 2e^- \tag{2.2}$$

$$2H^+ + 2e^- = H_2 \tag{2.3}$$

Eqs. (2.2) and (2.3) can further be expressed in term of Eq. (2.4)

$$Fe\,(metal) + 2H^{+}\,(ions) \;=\; Fe^{2+}\,(ion) + H_2\,(gas) \qquad (2.4)$$

The quantity of current that passes through this cell is proportional to the amount of metal that corrodes. One ampere per year will dissolve 20 lb of steel per year.

Anything that interferes with these reactions or the cell circuit could reduce corrosion. In pure water, hydrogen "bubbles" collect on the cathode, providing an insulating blanket that reduces current flow and practically stops corrosion. This is called polarization; because it occurs on the cathode, it is termed cathodic polarization. In strong acid solutions, the hydrogen is continuously evolved as bubbles breaking from corroding steel with the corrosion continuing unabated until either all the metal or acid is consumed.

2.4.1 Types of Corrosion [13]

There are a number of different kinds of corrosion, depending on the types of materials involved and the nature of the surrounding media, as shown in Figure 2.7.

Galvanic corrosion occurs when dissimilar metals are put together in the same electrically conductive medium. The metal that is more oxidation resistant becomes the cathode, while the less resistant metal is the anode and undergoes rapid corrosion.

Concentration cell corrosion occurs when the conductive fluid that surrounds the metal is not homogeneous. Cathodes and anodes form because of differences in ionic concentration between different regions of the medium. The resulting corrosion is highly localized and often results in pitting.

Pitting is a type of corrosion that may be described as a condition intermediate between general corrosion and passivity (no corrosion). With pitting the corrosion takes the form of many small holes over the surface of the metal.

Stress corrosion cracking is caused by a combination of internal stresses that occur during processing and corrosion. In this case corrosion proceeds very rapidly at

the spot where the stresses are concentrated and failure of the material may be very immediately.

Intergranular corrosion occurs at the grain boundaries of the metal due to the presence of impurities or stresses. Corrosion occurs on exposure of the metal's surface to a corrosive medium.

Uniform corrosion attacks the entire piece of metal. It can be caused by exposure to substances such as strong acid.

(a) (b) (c)

(d) (e) (f)

Figure 2.7 Types of corrosion: (a) Galvanic corrosion, (b) Concentration cell corrosion, (c) Pitting, (d) Stress corrosion cracking, (e) Intergranular corrosion and (f) Uniform corrosion attacks [14-19]

2.4.2 Corrosion Prevention [13]

There are mainly five approaches are used to prevent and reduce the rate of the corrosion:

- Protective coatings such as paint. Such a coating forms a barrier between the metal and its environment; therefore, current cannot flow.
- Cathodic protection. A direct current is impressed on the metal so that current enters
- Corrosion-resistant alloys. Metal ions do not readily form; therefore, corrosion does not occur.
- Addition of inhibitors. These may polarize one of the electrodes and thus interrupt the current flow.
- Very pure metals. These are homogeneous and have fewer tendencies to form anodes and cathodes.

2.4.3 Corrosion Theory [8]

The aqueous corrosion of metals requires the presence of an electrolyte at the metal surface, even if only as a thin film of electrolyte. Ions must migrate to maintain charge balance, as oxidation and reduction reaction occur on the metal surface. Typical oxidation reactions include the oxidation of a metal to either a soluble ionic form or an insoluble form as exemplified by the following reactions:

$$M \longrightarrow M^{n+} + ne^- \quad (2.5)$$

$$2M + 3H_2O \longrightarrow M_2O_3\,(s) + 6H^+ + 6e^- \quad (2.6)$$

A site at which such oxidation reactions occur is called an anode, and the oxidized products that form are usually influenced by pH value and other electrolyte constituents. The reduction reaction depends on environmental conditions, with the following common reactions:

$$O_2 + 2H_2O + 4e^- \longrightarrow 4OH^- \quad (2.7)$$

$$2H^+ + 2e^- \longrightarrow H_2 \quad (2.8)$$

A site at which such reduction reactions occur is called a cathode, and it is important to note that these reduction reactions result in a local increase in pH value. A corrosion cell composes of an anode and a cathode along with the electrolyte, with electron flowing from anode to cathode through the metal substrate and cation migrating from anode to cathode through the electrolyte to maintain and overall charge balance.

For a single redox reaction occurring at a noble metal electrode at a Pt, under conditions such that the current is limited only by the rate of electron transfer, the current density is given by the Butler-Volmer equation.

$$i = i_0 \left\{ \exp\left[\frac{(1-\alpha) nF\eta}{RT} \right] - \exp\left[\frac{-\alpha nF\eta}{RT} \right] \right\} = i_a - i_c \quad (2.9)$$

where;

i	= Current density (A cm^{-2})
i_o	= Exchange current density (A cm^{-2})
α	= Charge transfer coefficient
η	= Activation overpotential given by $\eta = E - E_{eq}$
n	= Number of electrons transferred
R	= Gas constant (8.314 J mol^{-1} K^{-1})
T	= Temperature (K)
F	= Faraday's constant (96,485Cmol^{-1} or J mol^{-1} V^{-1})

When $\eta = 0$, the potential E is the equilibrium potential E_{eq} (predicted by the Nernst equation) and the net current is zero. At this point, the individual components of the current (i_a and i_c) are equal and each is equal to i_o. As can be seen from Equation 2.9, when $\eta > 0$, $i_a > i_c$ and the net current is anodic (positive), whereas when $\eta < 0$, $i_a < i_c$ and the net current is cathodic (negative). The exchange current i_o is a measure of kinetic facility and a function of the heterogeneous electron transfer rate constant [97].

When two different redox reactions are occurring on the metal surface, the current is given by the equation.

$$i = i_{corr}\left\{ \exp\left[\frac{2.3(E-E_{corr})}{\beta_a}\right] - \exp\left[\frac{2.3(E-E_{corr})}{\beta_c}\right]\right\} \qquad (2.10)$$

where; i = Current density (A cm^{-2})

i_{corr} = Corrosion current (A)

E = Potential (V)

E_{corr} = Corrosion potential (V)

Anodic beta Tafel (β_a) and Catodic beta Tafel (β_c) are given by

$$\beta_a = \frac{2.3RT}{(1-\alpha)nF} \quad \beta_c = \frac{-2.3RT}{\alpha nF} \qquad (2.11)$$

Both β_a and β_c are having a value of 0.12 V at 25°C for a one electron transfer and for α = 0.5. Equation 2.10 is identical in form to Equation 2.9 and is valid when electron transfer is the only rate limiting process (i.e., ohmic polarization and concentration polarization are absent).

As (E - E_{corr}) → 0 (i.e., for small polarization), the exponential terms in Equation 2.10 may be expanded using a power series, and only the leading order terms retained, leading to the result

$$i = 2.3 i_{corr}(E-E_{corr})\frac{\beta_a + |\beta_c|}{\beta_a|\beta_c|} \qquad (2.12)$$

Differentiation of this expression leads to the Stern-Geary equation [99].

$$i_{corr} = \frac{\beta_a|\beta_c|}{R_p\, 2.3(\beta_a + |\beta_c|)} \quad \text{where} \quad R_p = \left[\frac{dE}{di}\right]_{E\to E_{corr}} \qquad (2.13)$$

R_p is called the polarization resistance and can be determined from the slope of the linear portion of the $i - E$ curve in the vicinity of the corrosion potential by using a polarization of only a few mV from E_{corr} (this method is known as the polarization resistance method). From the measured R_p value and the known (or estimated) β values, the corrosion current can be calculated from Equation 2.13. The corrosion rate is then determined from Faraday's law:

$$Corrosion = \frac{i_{corr} a}{nF} = \frac{m}{tA} \tag{2.14}$$

where; a = Atomic weight of the metal

m = Mass loss per unit time t

A = Area of the metal

Another approach to obtain i_{corr} and E_{corr} is to use the Tafel extrapolation method. Here a sufficiently large polarization from E_{corr} is used so that one or the other of the terms in Equation 2.14 is negligible. For a positive (or anodic) polarization when $(E - E_{corr}) > 0$, the second term in Equation 2.14 is negligible and the equation may then be rearranged to give an expression relating the anodic polarization (η_a) to the anodic current (i_a):

$$\eta_a = E - E_{corr} = \beta_a \log\left(\frac{i_a}{i_{corr}}\right) \tag{2.15}$$

Similarly, for negative (or cathodic) polarization when $(E - E_{corr}) < 0$, the first term in Equation 2.14 is negligible and the rearrangement then gives a corresponding expression relating the cathodic polarization (η_c) to the cathodic current (i_c):

$$\eta_c = E - E_{corr} = \beta_a \log\left(\frac{|i_a|}{i_{corr}}\right) \tag{2.16}$$

Equation 2.15 and Equation 2.16, called Tafel equations, explain the linear relationship between potential and log current observed when only the rate of electron-transfer limits the current.

The Tafel extrapolation method is illustrated in Figure 2.8. The solid curve represents the experimental polarization curve that would be observed, whereas the dashed lines are the extrapolations of the linear branches. The intersection of these extrapolated lines provides the corrosion potential (E_{corr}) and the corrosion current I_{corr}). The Figure 2.8 also illustrates the behavior when concentration polarization is present and the current is limited, partially or entirely, by the mass transfer of the oxidant to the metal surface.

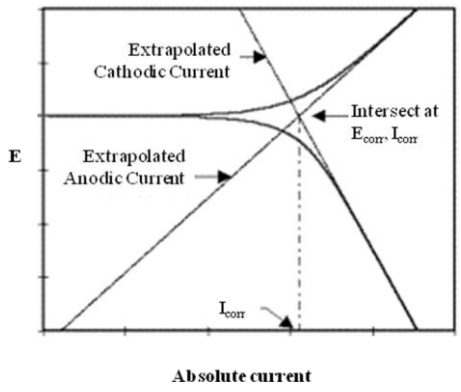

Figure 2.8 Polarization diagram illustrating the Tafel extrapolation method [8]

2.4.4 Corrosion mechanism [20]

Nanocomposite coatings present a different mechanism depending on the existence of surface crazing. Once the coating surface is broken, the metal substrate is exposed to corrosion process, and oxide surface thickness increase with the time. The adherence of the coating seems to be a determinant factor on the corrosion rate control.

The corrosion mechanism is represented in Figure 2.9. The diffusion of pollutants across the coating surface is the beginning of corrosion process, because zones with a poor adherence are the suitable points to be attacked by electrochemical corrosion reactions. The alkyd coating undergoes surface crazing after the pollutant diffusion and adherence loss processes. After the beginning, water and oxygen attack directly to the metal substrate yielding steel complexes from OH groups and oxygen. These compounds precipitate allowing only the selective access of water. The growth

of resultant bubble leads to fracture and disappearance of coating. The corrosion mechanism is represented in Figure 2.10.

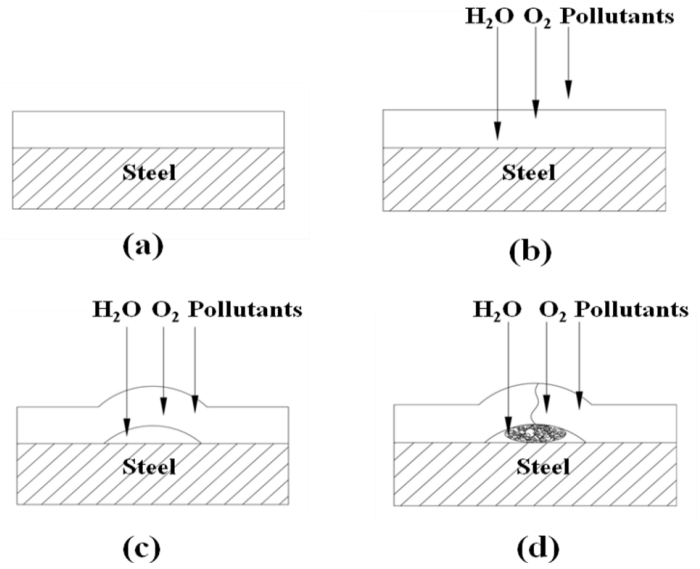

Figure 2.9 Degradation mechanism of alkyd coatings; (a) initial state of the surface, (b) pollutants access, (c) pollutants diffusion and (d) corrosion products obtained under the surface [20]

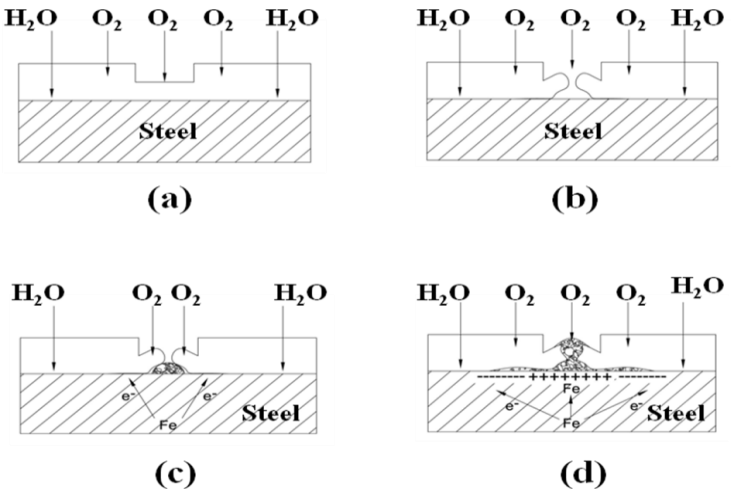

Figure 2.10 Degradation mechanism of alkyd coatings; (a) initial state of the surface, (b) pollutants access, (c) pollutants diffusion and (d) corrosion products obtained under the surface [20]

2.5 Literature Reviews

Ali *et al*. [7] studied the preparation of PANI/MMT nanocomposites at 5 wt% of MMT with hydrophilic and organophilic nanoclay particles by *in situ* polymerization. The nanocomposites were characterized using FT-IR, D.C. electrical conductivity measurement and cyclic voltammetry techniques. The anticorrosive properties of a 100 μm thickness coating of nanocomposites on iron coupons were evaluated and compared with pure polyaniline coating. Results of the corrosion studies showed that the anticorrosive property of both hydrophilic and organophilic PANI/MMT nanocomposite coatings on iron samples was better than for pure polyaniline coating.

Binitha *et al*. [21] studied the preparation and characterization of exfoliated PANI/MMT nanocomposites. Exfoliated nanocomposites preparation is an evolving and challenging area where in the present work exfoliated PANI/clay nanocomposites have been successfully prepared by *in situ* polymerization of aniline onto pre-exfoliated transition metal ion exchanged montmorillonite clays. XRD patterns clearly showed exfoliation of clay layers in the polymer matrix on the nanoscale. Present method is a promising alternative method for the preparation of nanocomposites from polyaniline when compared to the complicated and less economical product for the same from organically modified clays.

Soundarajah *et al*. [22] investigated mechanical properties of PANI/O-MMT nanocomposites. The PANI/O-MMT nanocomposites were prepared by *in situ* intercalative polymerization. Various compositions with different clay contents were prepared with a constant polymer concentration. The mechanical properties including Young's modulus, fracture toughness, hardness and impact energy of polyaniline significantly increased by the presence of MMT clay in the nanocomposites of PANI and MMT up to 23 wt% of MMT and decreased at higher clay contents. Therefore, the 23 wt% of PANI-MMT nanocomposites that had the optimum mechanical characteristics could be suggested for applications, such as surface coating and corrosion protection.

Patrycja *et al*. [23] studied the preparation and conductivity of PANI-MMT composites. The PANI-MMT composites were prepared in two different methods.

First method is polymerization of aniline hydrochloride with ammonium peroxydisulfate (APS) in aqueous suspensions of MMT. The second method is the intercalation of aniline hydrochloride into MMT in aqueous suspension followed by the oxidation with APS. The PANI-MMT composites were analyzed by FT-IR, TGA, SEM, XRD and Raman spectroscopies. The results indicated that the PANI coatings of MMT determine the overall conductivity of composites. For that reason, both types of composites behaved similarly. The loading above 30 wt% PANI provided the conductivity of composites in the range 10^{-2} to 10^{0} Scm^{-1}.

Ebrahimi *et al*. [24] investigated the synthesis of exfoliated polyaniline-clay nanocomposites in supercritical CO_2. The fully exfoliated polyaniline-clay nanocomposites (PCNs) with high purity via *in situ* polymerization of aniline in Cloisite 30B nano-clay suspension in supercritical CO_2 ($ScCO_2$) medium were synthesized. The Cloisite 30B was first delaminated with $ScCO_2$ treatment in the presence of aniline monomers. Ammonium peroxydisulfate (APS) solution was added rapidly into the mixture of delaminated Cloisite 30B and aniline monomers to produce PCNs. The products were analyzed by FT-IR, XRD, UV-vis spectroscopy and SEM. The SEM results indicated good dispersion properties and high homogeneity of the $ScCO_2$ synthesized nanocomposites compare to atmospheric synthesized one. FTIR and UV-vis spectroscopy revealed that no effect on the chemical structures of the PANI was observed by using supercritical CO_2. Measurement of conductivity showed that, although Cloisite 30B was an insulator, it have no significant effect on the conductivity of nanocomposites. The conductivity of nanocomposites was slightly lower than pristine PANI and decreased by nano-clay loading.

Rosa *et al*. [25] studied the preparation of polyaniline (PANI) and poly-ortho-methoxyaniline (POMA) by chemical method, with different synthesis conditions. Two solutions were prepared, one with the oxidizing agent ammonium persulfate and the other monomer including aniline or ortho-methoxyaniline. The polymeric film deposited on carbon steel, showed good adherence and homogeneous thickness. However, they showed differences in surface morphology, being fibrilar for PANI and rough for POMA. The results indicated that modified carbon steel present a decrease in their dissolution within the corrosive medium due to the morphological

differences of the polymeric films. PANI film showed better protective properties than the POMA films.

Kamaraj *et al*. [26] studied the effect of benzoate doped polyaniline on the corrosion protection of iron by polyaniline-vinyl coatings in acid and neutral media. Polyaniline was obtained by oxidative polymerization of aniline in HCl using ammonium persulfate oxidant. The synthesized polyaniline was dedoped by 1 M NH_4OH and re-doped by 1 M benzoic acid. The polyaniline containing paint was prepared using vinyl resin with 1 wt% PANI as pigment. The corrosion protection performance of vinyl coating on steel with 1 wt% polyaniline was studied by Electrochemical Impedance Spectroscopy (EIS). The vinyl coating containing benzoate doped polyaniline was able to protect steel in neutral media better than in acid media due to passivating ability of benzoate ions in neutral solution.

Venkatachari *et al*. [27] investigated the corrosion resistant property of the polyaniline blended coating. The polyaniline doped by phosphate prepared by chemical oxidative method using ammonium persulfate as oxidant. The epoxy coating with the phosphate doped polyaniline was able to offer protection in saline and acid media. The coating was able to protect the steel more in 3 %(w/w) NaCl and 0.1 N H_3PO_4 than in 0.1 N HCl.

Radhakrishnan *et al*. [28] studied the conducting polyaniline-nano-TiO_2 composites for smart corrosion resistant coatings. The conducting PANI nano-particulate TiO_2 hybrid composites prepared by *in situ* polymerization were used for coating with PVB as the matrix. The effect of addition of nano-TiO_2 on the improvement of has been clearly brought out. The novelty of these coatings lies in generation of corrosion inhibition by three mechanisms operating simultaneously viz. improvement of barrier properties, redox behavior of PANI and formation of p-n junctions preventing easy charge transport when coating was threatened to be destroyed due to scratch or scribble. Apart from the prevention of corrosion, these coatings had good gloss and shiny surface, which was not easily obtained in conventional coating, prepared with commercial micron size particle additives. Such systems could be used as a primer coat or even as a single coating on steel where color was not a very important.

CHAPTER III

EXPERIMENTAL

3.1 Chemicals

1. Aniline, AR grade : Loba Chemie
2. Montmorillonite clay (Cloisite®15A) : Southern Clay Products
3. Hydrochloric acid, 37%, AR grade : QRec
4. Ammonium persulfate, AR grade : Ajax Finechem
5. Methanol, AR grade : QRec
6. Ammonia solution, 25%, AR grade : QRec
7. 1-Methyl-2-pyrrolidone, AR grade : QRec
8. Sodium hydroxide, AR grade : QRec
9. Sodium chloride, AR grade : CARLO ERBA
10. Sulfuric acid, 98%, AR grade : QRec
11. Acetone, AR grade : QRec
12. Nitrogen gas, 99.9% : Praxair
13. De-ionized water

3.2 Equipments

1. Fourier Transform Infrared Spectrophotometer (FT-IR) : Spectrum GX Perkin Elmer
2. UV-Visible Spectrophotometer (UV-Vis) : Shimadzu Model UV-1800
3. X-ray Diffractometer (XRD) : Bruker AXS Model D8
4. Thermal Gravimetric Analyzer (TGA) : Perkin-Elmer Pyris Diamond
5. Scanning Electron Microscope (SEM) : JEOL JSM-6400
6. Potentiostat/Galvanostat Instrument : Autolab Type III
7. Salt Spray : Q-FOG

3.3 Synthesis of Polyaniline and PANI/MMT nanocomposites by *In Situ* Chemical Oxidation Polymerization

Polyaniline was prepared by *in situ* chemical oxidation polymerization. Aniline polymerization was performed in 1M HCl solution by using ammonium persulfate ($(NH_4)_2.S_2O_8$) as oxidant/initiator. The reaction mixture was vigorously stirred at 0°C to 5°C for 6 h. The emeraldine salt precipitate was obtained by filtration followed by washing with 80/20 distilled water/methanol (v/v) mixture and drying in vacuum oven at 50°C for 48 h, the schematic diagram of PANI and PANI/MMT nanocomposite synthesis as shown in Figure 3.1. The emeraldine salt form of polyaniline was dedoped with 1M ammonia solution for 4 h followed by washing with 80/20 distilled water/methanol mixture and drying in vacuum oven at 50°C for 48 h. The obtained emeraldine base is dark brown powder. 1 gram of the emeraldine base form of polyaniline was dissolved in 40 mL of 1-methyl-2-pyrrolidone solvent under magnetically stirred condition at room temperature for 7 h. The resulting viscous solution was filtered to remove any insoluble particles, the schematic diagram of coating solution of PANI and PANI/MMT as shown in Figure 3.2. The PANI/MMT nanocomposites were prepared by similar procedure with montmorillonite addition. The effects of montmorillonite loading were studied over the range of 0, 1, 3, 5 and 7 %wt based on monomer content.

The monomer conversion was determined by gravimetric calculation as follows:

$$Monomer\,Conversion(\%) = \frac{M_0 - M_1}{M_2} x100 \qquad (3.1)$$

Where M_0 = Mass of the resulting composite particles (gram)

M_1 = Mass of the charged MMT particles (gram)

M_2 = Mass of the charged aniline monomer (gram)

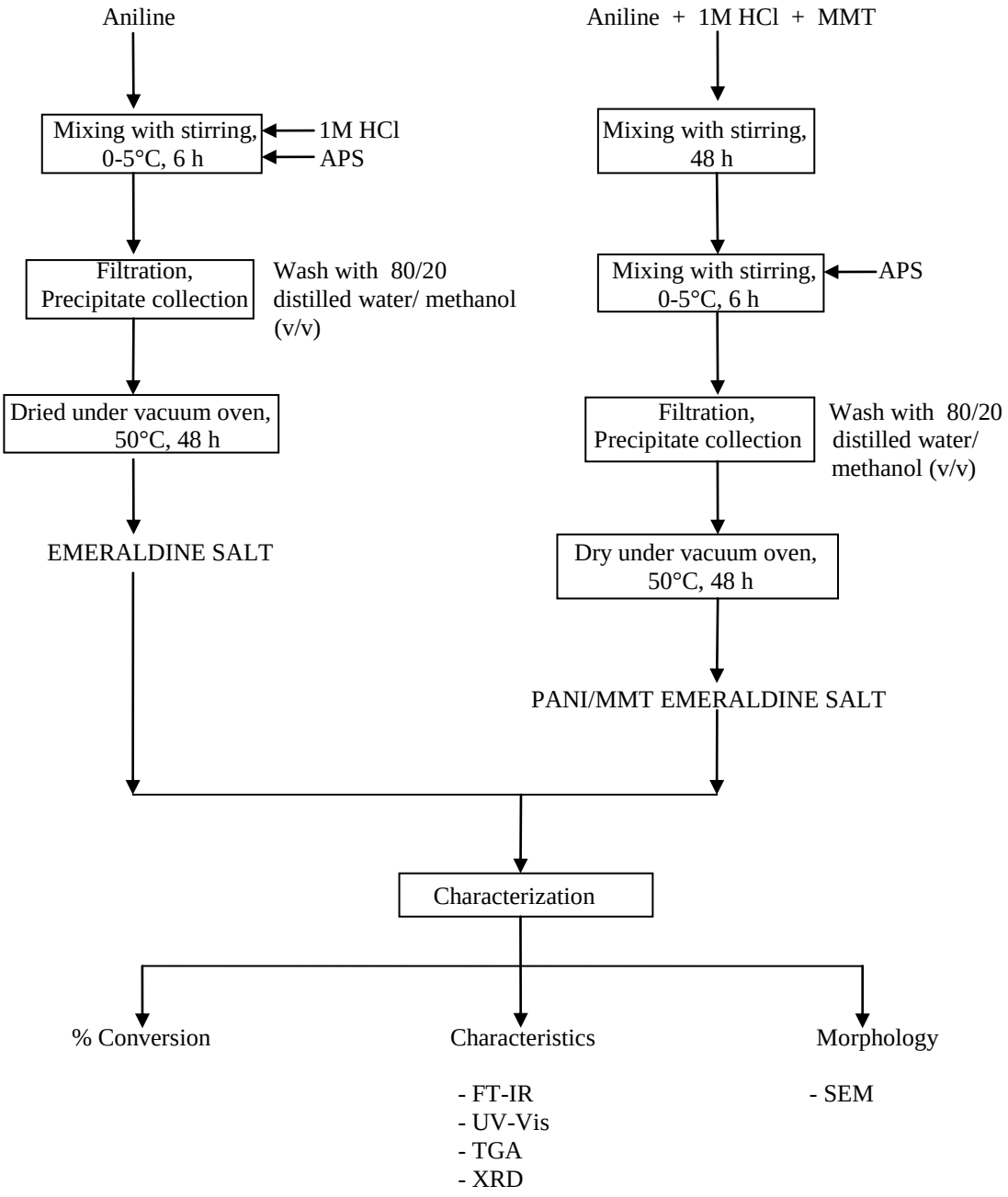

Figure 3.1 The schematic diagram of PANI and PANI/MMT nanocomposites synthesis

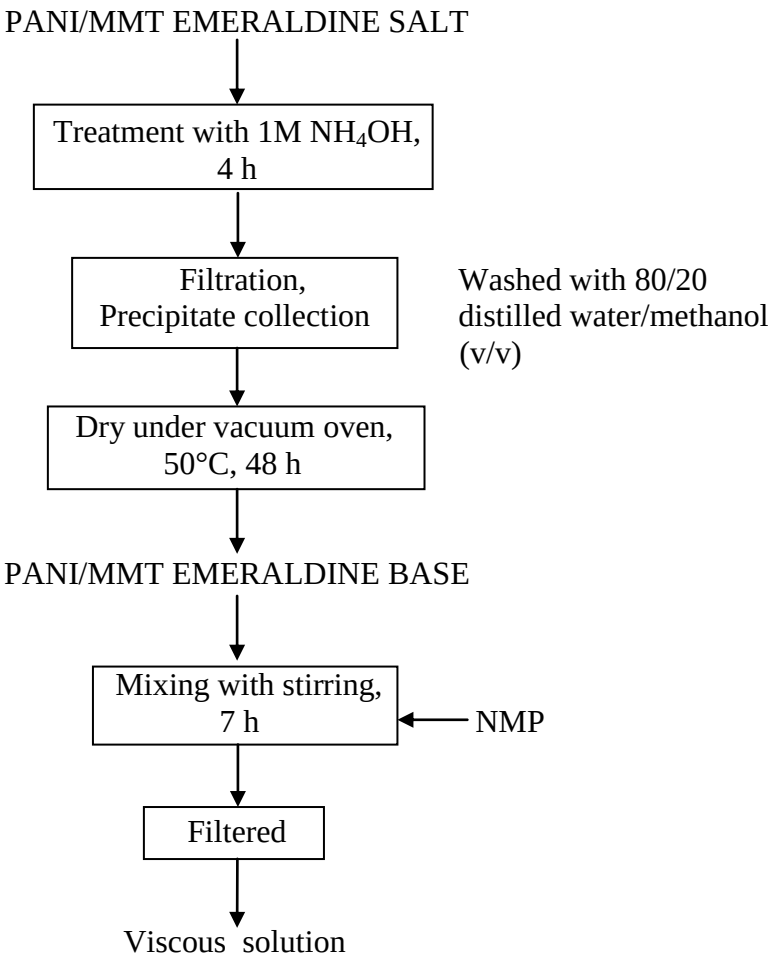

Figure 3.2 The schematic diagram of coating solution of PANI and PANI/MMT

3.4 Coating of PANI/MMT on steel samples

Steel Spring Sheet (SK5) coupons with 1 cm × 1 cm × 0.1 cm and 2 cm × 5 cm × 0.1 cm in dimensions were used in corrosion studies. In order to remove any existing passive film, the steel coupons were mechanically polished using 150 and 400 grade emery papers followed by rinsing with distilled water and acetone prior to coating and corrosion experiments. The coating was deposited by high-pressure air spray system (Figure 3.3(a) and (b)). The film was then allowed to dry in vacuum oven at 40°C. The effect of film thickness (10, 20, 30, 40 and 50 μm) on steel was studied. The thickness was measured using electronic outside micrometer. The measurement was taken from three different points distributed over the sample, and the reported values were averaged of three measurements.

(a) (b)

Figure 3.3 (a) Spray gun and (b) Steel coupons coated by spray method

3.5 Characterization Methods

3.5.1 Fourier Transform Infrared (FT-IR) Spectroscopy

Structures of polyaniline and PANI/MMT nanocomposites were characterized using a Spectrum GX Perkin Elmer in the range of 400-4000 cm^{-1}. The samples were prepared by dispersed in potassium bromide (KBr) and compressed into pellets.

3.5.2 UV-Visible Spectrophotometer

The UV-Visible Spectra were obtained in a UV-Visible Spectrophotometer scanning in the wavelength range 200-800 nm. The samples were dissolved in 1-methyl-2-pyrrolidone solvent.

3.5.3 Thermogravimetric Analysis (TGA)

Thermogravimetric analysis (TGA) was performed using a Perkin-Elmer Pyris Diamond TG/DTA. The samples were heated from 40°C to 700°C with heating rate of 10°C/min under nitrogen atmosphere. The initial decomposition temperature (T_{id}) and the temperature at the maximum mass loss rate (T_{max}) were recorded.

3.5.4 X-ray Diffraction (XRD)

X-ray diffraction (XRD) measurements were performed using a Bruker AXS Model D8 Discover with CuKα X-ray radiation (1.5406 Å) at 40 kV and 40 mA. The samples were scanned in the 2θ range from 1° to 35°, with a step time of 0.3 s and a step size of 0.02°. The measurements were operated by Evaluation (EVA) program.

3.5.5 Morphological Study

The morphology of nanocomposites was investigated by scanning electron microscope (SEM, JEOL Model JSM-5410 LV). Samples were placed on a SEM stub and the particles were arranged in a single layer, not clustered. For cross section morphology of the polymeric films of PANI/MMT nanocomposites, a steel sample was placed in a PVC ring form. The sample should be dry as moisture in the sample can interfere with polymerization of acryric and affect adhesion. The steel sample was completely immersed in acrylic and phenolic resins, and cured for 7 minutes under the temperature of 180 ^{o}C and pressure of 30 kPa. The sample in hardened resin was removed from the mold, and sectioned. After that, the sectioned sample was polished by polishing cloths, washed by ethanol and dried.

3.5.6 Corrosion Study

The electrochemical Tafel slope analysis was used to evaluate the anticorrosive performance of PANI/MMT nanocomposites coating on steel samples. Tafel plots for polyaniline and PANI/MMT coated steel samples were recorded by sweeping the potential from equilibrium potential toward negative and positive potentials against Ag/AgCl reference electrode in 1M H_2SO_4 electrolyte.

Figure 3.4 The electrochemical Tafel slope analysis apparatus

The corrosion resistance of coated steel samples was measured according to the standard testing method ASTM B117 using salt spray tester. Salt spray test was an accelerated corrosion test that produces a corrosive attack to the coated samples in order to predict its suitability in use as a protective finish. The appearance of corrosion products was evaluated after a period of time. The apparatus for testing consists of a closed testing chamber, where a corrosive environment of dense saline fog was produced. The samples exposed in the chamber were subjected to severely corrosive conditions, and were tested continuously for the duration 96 h with 5 wt% NaCl solution. The period in testing without showing signs of corrosion increased with increasing the corrosion resistance of the coating.

CHAPTER IV

RESULTS AND DISCUSSION

Polyaniline (PANI) and Polyaniline/montmorillonite (PANI/MMT) nanocomposites were successfully synthesized by *in situ* chemical oxidative polymerization using ammonium persulfate as an oxidant/initiator. The reaction mixture was vigorously stirred at 0°C to 5°C for 6 h. The monomer conversion PANI/MMT nanocomposites were determined. The PANI and PANI/MMT nanocomposites were also characterized by Fourier-transform infrared spectroscopy (FT-IR) and X-ray diffraction (XRD). The surface morphology of nanocomposites was observed by scanning electron microscopy (SEM). Thermal properties of the PANI/MMT nanocomposites were examined by thermogravimetric analysis (TGA). The electrochemical Tafel slope analysis and salt spray test were used to evaluate the anticorrosive performance of PANI/MMT nanocomposites coating on steel samples.

4.1 Synthesis of Polyaniline and PANI/MMT Nanacomposites by *In Situ* Chemical Oxidative Polymerization

The effect of montmorillonite loading on monomer conversion is presented in Table 4.1. The MMT loading had a significant effect on monomer conversion. The effect of MMT loading was studied over the range of 1 - 7 wt% based on monomer weight. Monomer conversion slightly decreased with an increasing in MMT loading. It is also possible that the aggregation of MMT particles tended to decrease the number of monomer-swollen micelles and particle stability. Furthermore, at high loading of MMT, the high viscous liquid of PANI/MMT nanocomposites was obtained which implied to the decreasing in monomer conversion. Thus, the highest monomer conversion of PANI/MMT nanocomposites was achieved at 75.8% with an appropriate MMT loading of 1 wt%.

Table 4.1 Effect of montmorillonite content on monomer conversion and standard deviation.

Samples	MMT Content (%wt based on monomer)	Conversion (%)	Standard deviation
PANI	0	78.5	1.35
PANI/MMT(1%wt)	1	75.8	3.68
PANI/MMT(3%wt)	3	74.0	3.49
PANI/MMT(5%wt)	5	73.3	3.81
PANI/MMT(7%wt)	7	73.4	1.55

4.2 Characterization of PANI/MMT Nanocomposites

4.2.1 FT-IR Analysis

FTIR spectra of PANI, MMT and PANI/MMT nanocomposites (3 wt% MMT) are shown in Figures 4.1. For the FTIR spectrum of PANI (Figure 4.1(a)), the peaks at 1578 and 1475 cm^{-1} attributed to C=N stretching of quinoid ring [9] and C=C stretching of benzenoid ring, respectively. The peak at 1297 cm^{-1} is assigned to the C-N stretching of benzenoid ring. Peaks at 1107 and 798 cm^{-1} correspond to C-H out-of-plane bending of 1, 2, 4-ring and C-H out-of-plane bending of 1, 2-ring, respectively [29].

For the FTIR spectrum of MMT (Figure 4.1(b)), the peaks at 3634, 3428, 2922, 2850, 1640, 1469, 1051 and 526 cm^{-1} are assigned to O-H stretching, O-OH stretching, C-H stretching of methyl and methylene group, RCONHR of ammonium salts, CH_3 deformation, Si-O stretching and Al-O stretching, respectively [29]. Figure 4.1(c) indicated that the main characteristic peaks of PANI and MMT presented in FTIR spectra of PANI/MMT nanocomposites.

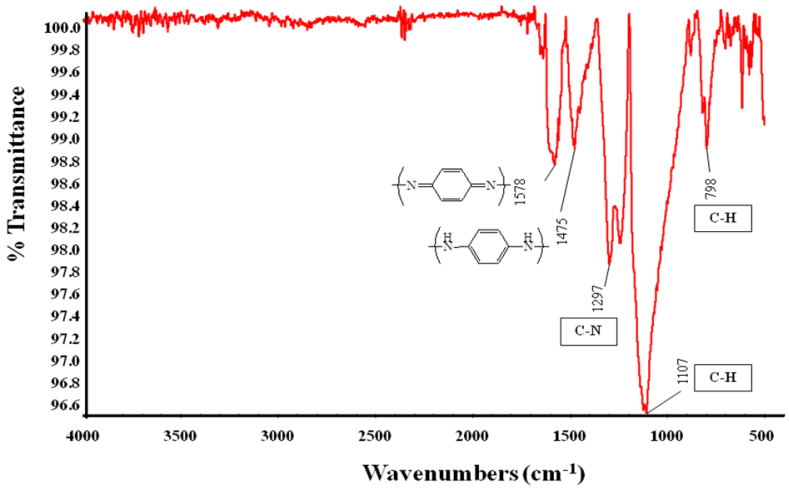

(a) PANI

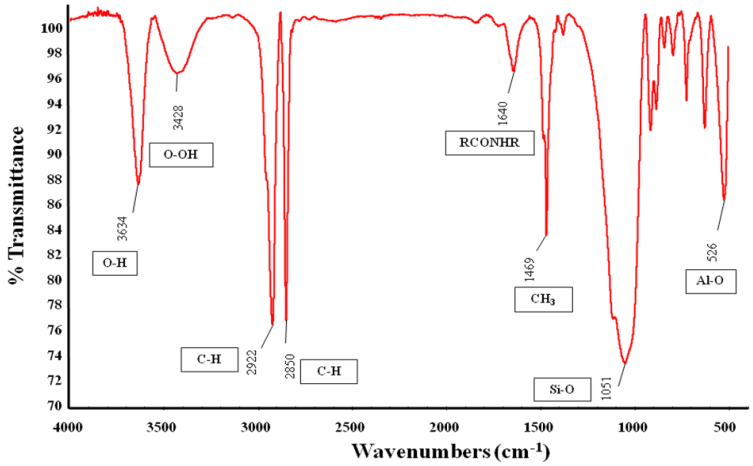

(b) MMT

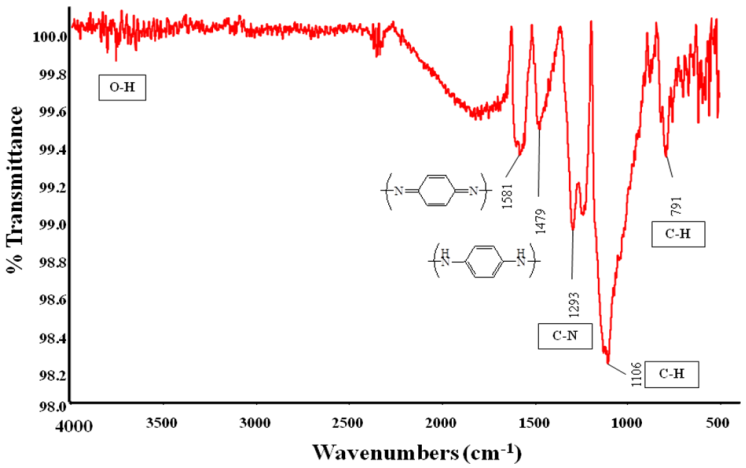

(c) PANI/MMT nanocomposites (3 wt% MMT)

Figure 4.1 FTIR spectra of (a) PANI, (b) MMT and (c) PANI/MMT nanocomposites (3 wt% MMT)

4.2.2 UV-VIS Analysis

For the UV-Visible spectrum of PANI shown in Figure 4.2, the characteristic peaks of PANI appeared at 330 and 630 nm attributed to emeraldine base PANI characteristic. The absorption peak at 330 nm corresponded to the π-π* transition in the benzenoid ring and the peak at 630 nm corresponded to the donor-acceptor interaction of quinoid ring [25].

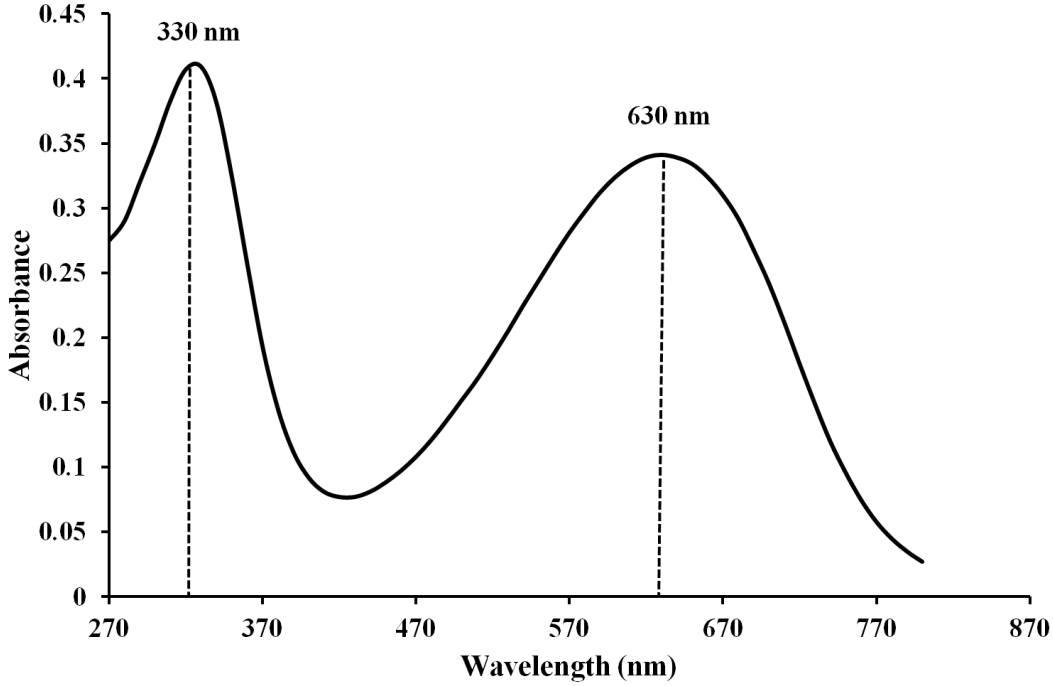

Figure 4.2 UV-Visible Spectrum of PANI

4.2.3 Thermogravimetric Analysis

Figures 4.3a and 4.3b illustrate the TGA curves and derivative curves (DTG curves) for MMT, PANI and PANI/MMT nanocomposites at 1, 3, 5 and 7 wt% of MMT loading. The MMT loading affected the decomposition temperature of PANI/MMT nanocomposites as presented in Table 4.2. The thermogram of MMT shows three-step decomposition. The first and second steps corresponded to decomposition of the organic matters present in the organo-modifier (desurfactant), the onset occurs near 200°C with two maxima at 247°C and 310°C. The last step is dehydroxylation of the MMT layer at 387°C. The similar result was earlier reported for characterization of systematically selected organo-montmorillonites [30].

The thermograms of PANI and PANI/MMT nanocomposites at 1, 3, 5 and 7 wt% MMT loading showed three-step polymer degradation and provided smooth weight loss curves. For PANI/MMT at 7 wt% MMT, the first step corresponded to the decomposition of the moisture, the onset occurs near 50°C with maximum at 82°C. The second step corresponded to the decomposition of organic compounds, the onset occur near 232°C with maximum at 287°C and the third step corresponded to the decomposition of the MMT layer and the polymer backbone chain breakage, the onset occurs near 560°C which was high compared with initial degradation temperature (T_{id}) of PANI (491.3°C).

Previous work reported that the unparalleled ability of MMT was found to improve the thermal stability of polymer matrix [30]. For the present work, it was found that T_{id} increased with an increasing in MMT loading. The thermal stability of the PANI/MMT nanocomposites were enhanced which could be attributed to the barrier improvement by MMT. MMT nanosheets acted as barriers which led to the hindered diffusion of volatile composition products within the nanocomposites [5]. Therefore, the MMT platelets gained a shielding effect and slow down the decomposition rate of nanocomposites.

Table 4.2 Degradation temperatures (°C) and weight loss (%) of PANI and PANI/MMT nanocomposites.

Sample	Loss of water			Loss of organic compounds			Polymer chain breakage		
	%wt Loss	T_{id} (°C)	T_{max} (°C)	%wt Loss	T_{id} (°C)	T_{max} (°C)	%wt Loss	T_{id} (°C)	T_{max} (°C)
PANI	5.1	51.1	86.3	13.8	236.2	320	16.9	491.3	610.1
PANI/MMT (1 wt%)	5.3	48.7	82.8	18.2	232.8	273.2	37.1	493.5	542.5
PANI/MMT (3 wt%)	5.3	59.2	80.0	16.7	232.0	293.9	32.7	511.7	554.7
PANI/MMT (5 wt%)	5.2	50.0	78.9	16.3	229.0	274.2	30.4	517.8	554.5
PANI/MMT (7 wt%)	5.7	51.4	80.5	19.0	228.0	274.0	36.4	560.0	577.0

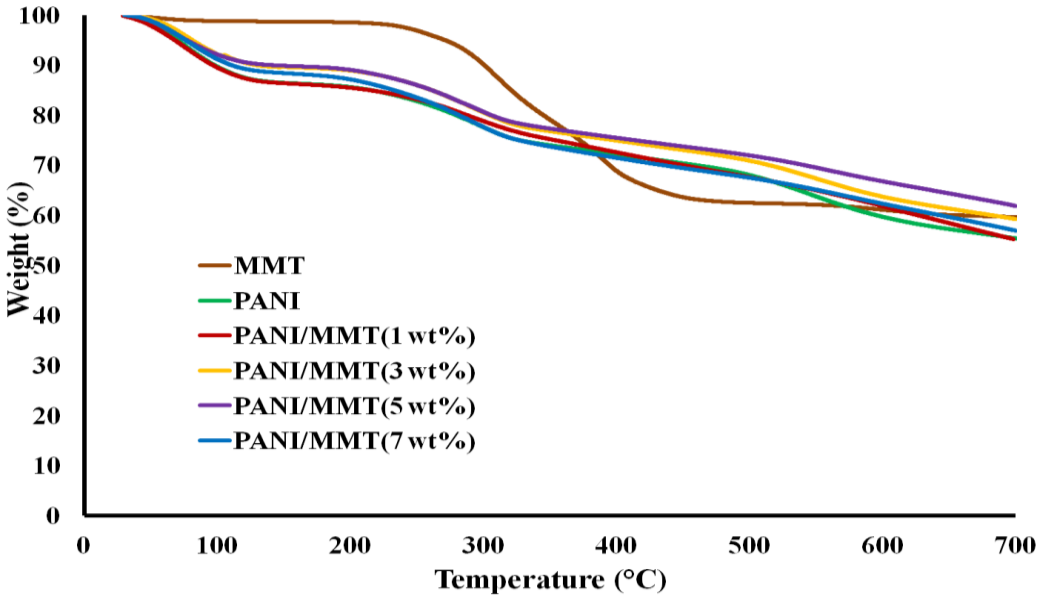

(a)

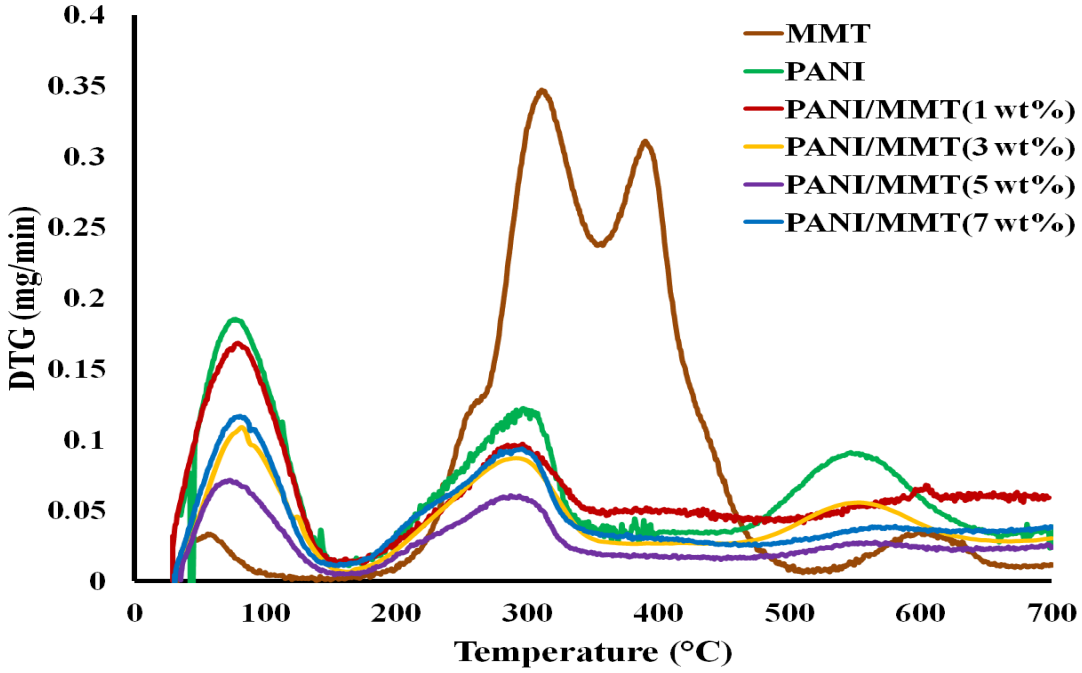

(b)

Figure 4.3 (a) TGA and (b) DTG curves of PANI/MMT nanocomposites with various MMT loading

4.2.4 XRD Analysis

Figure 4.4 presents the XRD patterns obtained from PANI, MMT and PANI/MMT nanocomposites at 1, 3, 5 and 7 wt% MMT loading. The spectrum of MMT showed a diffraction peak at 2θ of 2.81° corresponding to layer spacing (*d*-spacing) d_{001} of 3.14 nm. The similar result was reported in production bulletin of Cloisite15A from Southern Clay Products that d_{001} of MMT is 3.63 nm [32]. The XRD patterns of the PANI/MMT nanocomposites presented the principal PANI base peaks as well as MMT peaks. At room temperature, the d_{001} of the MMT is greater than that of the PANI/MMT nanocomposites (Table 4.3). This is due to the excessive hydration of simple inorganic cations in MMT and the lesser degree of hydration of the hydrophobic organic cations present within the interlayer space under ambient laboratory condition (25°C), as shown in Figure 4.5(a). In addition, the excessive PANI in MMT might cause a tightening of the MMT layers, resulting in a reduction of d_{001} layer spacing, as shown in Figure 4.5 (b). For the low MMT content of the PANI/MMT nanocomposites, the peak at 2.81° showed broadening and displacement, characterizing the intercalation of PANI in the MMT [33]. The similar trend results were earlier reported by Soundararajah Q.Y. *et al*. [22]. The PANI/MMT nanocomposites with lowest clay content (1 wt%) showed a similar XRD pattern to pure PANI which indicated to the exfoliated structure while the others have either a region of intercalated structure or a region of agglomeration [22]. Moreover, the driving force of polymerization of nanocomposites with low MMT content is much higher than to overcome the attractive electrostatic force between the negatively charged silicate layers and the interlayer cations that leads to exfoliation.

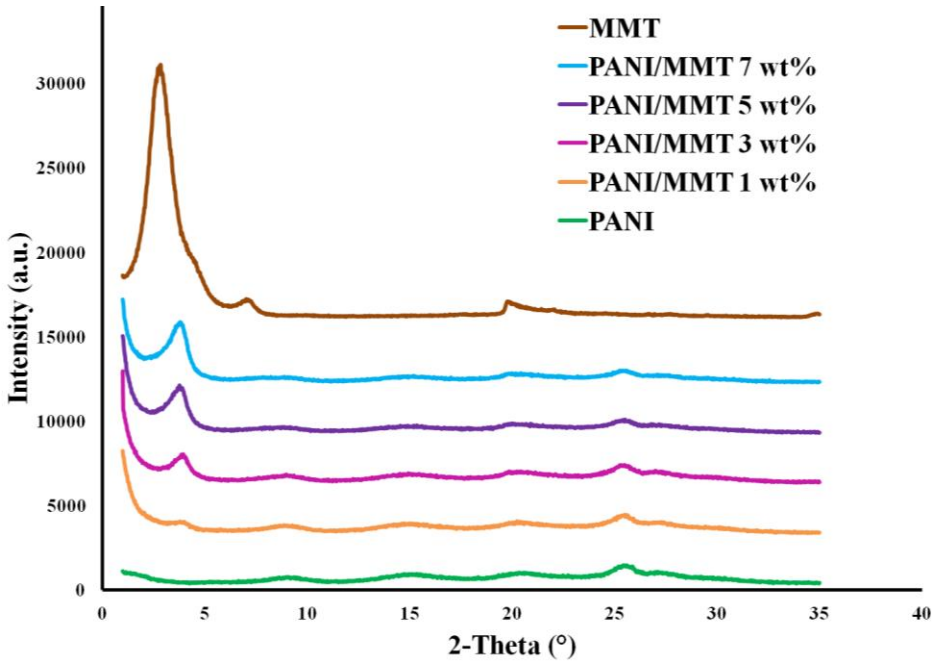

Figure 4.4 XRD patterns of montmorillonite, polyaniline and PANI/MMT Nanocomposites

Table 4.3 2θ and *d*-spacing of XRD spectra of PANI, MMT and PANI/MMT nanocomposites at 1, 3, 5 and 7 wt% MMT loading

Samples	**2θ (degree)**	**d_{001} (nm)**
PANI	25.45	0.35
MMT	2.81	3.14
PANI/MMT 1 wt%	3.79	2.33
PANI/MMT 3 wt%	3.56	2.48
PANI/MMT 5 wt%	2.88	3.07
PANI/MMT 7 wt%	3.06	2.88

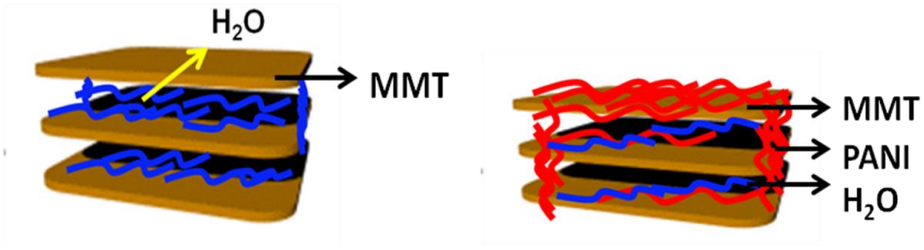

(a) **(b)**

Figure 4.5 Nanocomposites layers; (a) an excessive hydration in MMT and (b) the tightening of the MMT layers by excessive PANI in MMT

4.2.5 Morphology of Polyaniline and PANI/MMT Nanacomposites

The surface morphology of MMT was characterized by SEM as shown in Figure 4.6. The MMT particles seem to be stack together due to moisture. The thickness of MMT was 20-30 nm and the length was about 100-200 nm.

The morphologies of PANI and PANI/MMT nanocomposites examined by scanning electron microscopy (SEM) are shown in Figure 4.7. The morphology of PANI (Figure 4.7(a)) was similar to that prepared by chemical oxidative polymerization reported by Ali Olad *et al*. [2].

From Figure 4.7(a), the PANI illustrated agglomerated spheres. For the PANI/MMT nanocomposites at 1, 3, 5 and 7 wt% of MMT (Figures 4.7(c)-(f)), the MMT layers and the agglomerated spheres of PANI dispersion on the nanocomposites surface were observed. However, PANI with 7 wt% of MMT loading had more stacking than that at 1, 3 and 5 wt% of MMT loading.

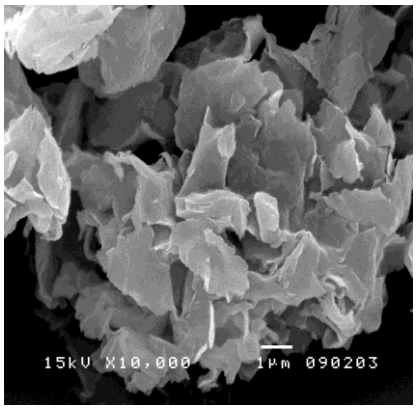

Figure 4.6 Scanning electron micrographs of MMT (10,000x magnification)

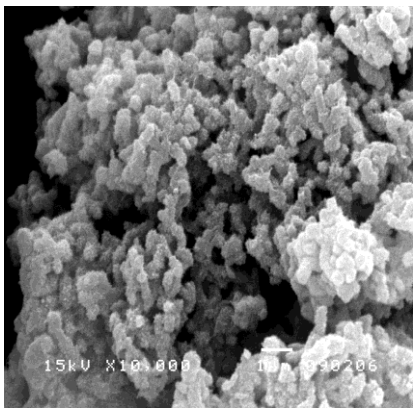

(a) PANI

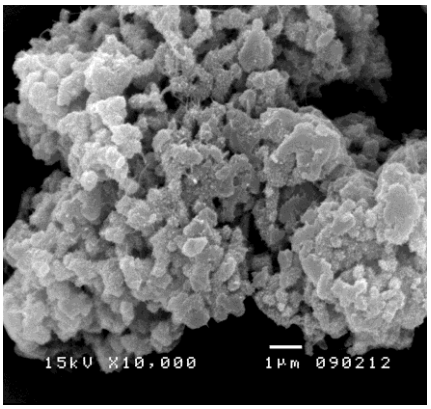

(b) PANI/MMT 1 wt%

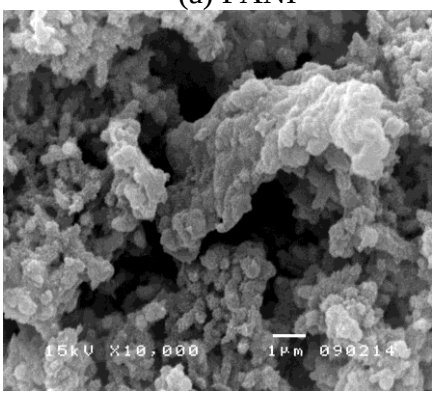

(c) PANI/MMT 3 wt%

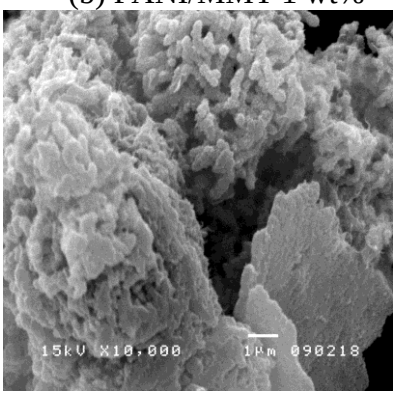

(d) PANI/MMT 5 wt%

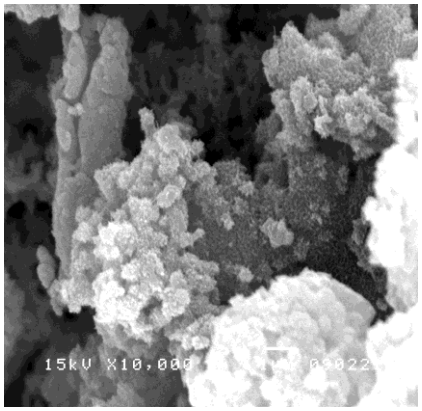

(e) PANI/MMT 7 wt%

Figure 4.7 Scanning electron micrographs of (a) PANI, (b) PANI/MMT 1 wt%, (c) PANI/MMT 3 wt%, (d) PANI/MMT 5 wt% and (e) PANI/MMT 7 wt% (10,000x magnification).

4.3 Corrosion Studies

4.3.1 Tafel Slope Analysis

The electrochemical Tafel slope analysis was used to evaluate the anticorrosive performance of PANI and PANI/MMT nanocomposites coating on steel samples. Tafel plots for PANI and PANI/MMT nanocomposites coated steel samples were recorded by sweeping the potential from equilibrium potential toward negative and positive potentials against Ag/AgCl reference electrode in 1M H_2SO_4 electrolyte. Figures 4.8 and 4.9 show the Tafel plots for PANI and PANI/MMT nanocomposites at 1, 3, 5 and 7 wt% MMT content coated steel samples with 10-50 μm thickness in 1M H_2SO_4 solutions. It was found that the corrosion current decreased with an increasing in film thickness, as shown in Figure 4.8. In addition, the effect of MMT loading on corrosion current at various film thickness were illustrated in Figure 4.9. For PANI and PANI/MMT coated at 10-50 μm thickness, the corrosion current decreased with increasing MMT loading.

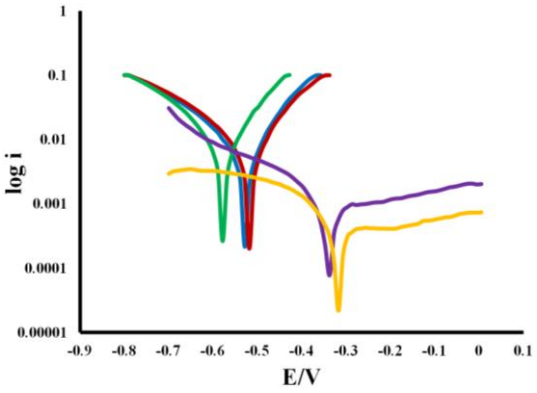

(a) PANI

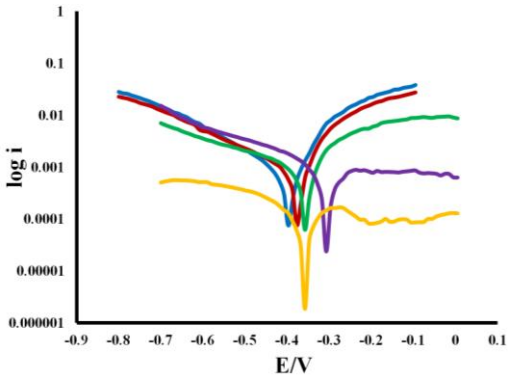

(b) PANI/MMT 1 wt%

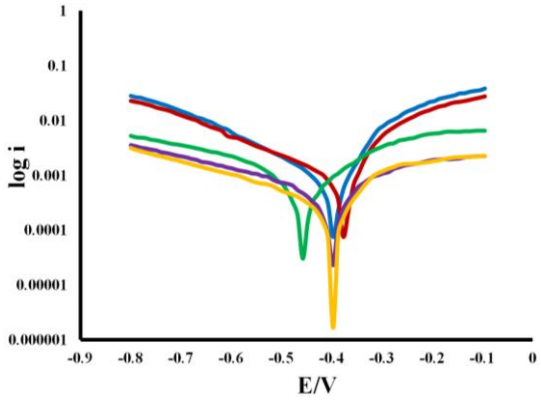

(c) PANI/MMT 3 wt%

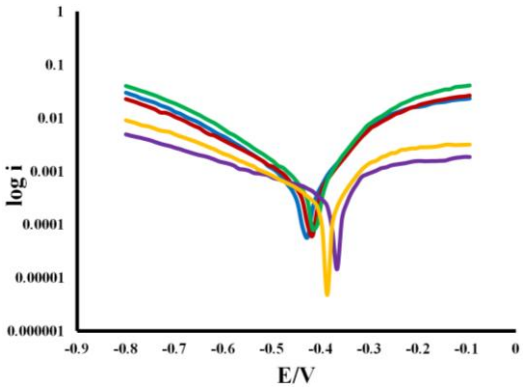

(d) PANI/MMT 5 wt%

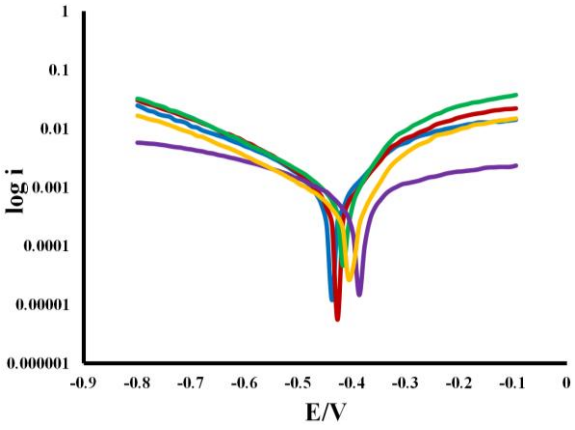

(e) PANI/MMT 7 wt%

Figure 4.8 Scanning Tafel plots for PANI and PANI/MMT nanocomposites coated steel samples in 1M H_2SO_4 solution; (a) PANI, (b) PANI/MMT 1 wt%, (c) PANI/MMT 3 wt%, (d) PANI/MMT 5 wt% and (e) PANI/MMT 7 wt%; (——) 10 µm, (——) 20 µm, (——) 30 µm, (——) 40 µm and (——) 50 µm

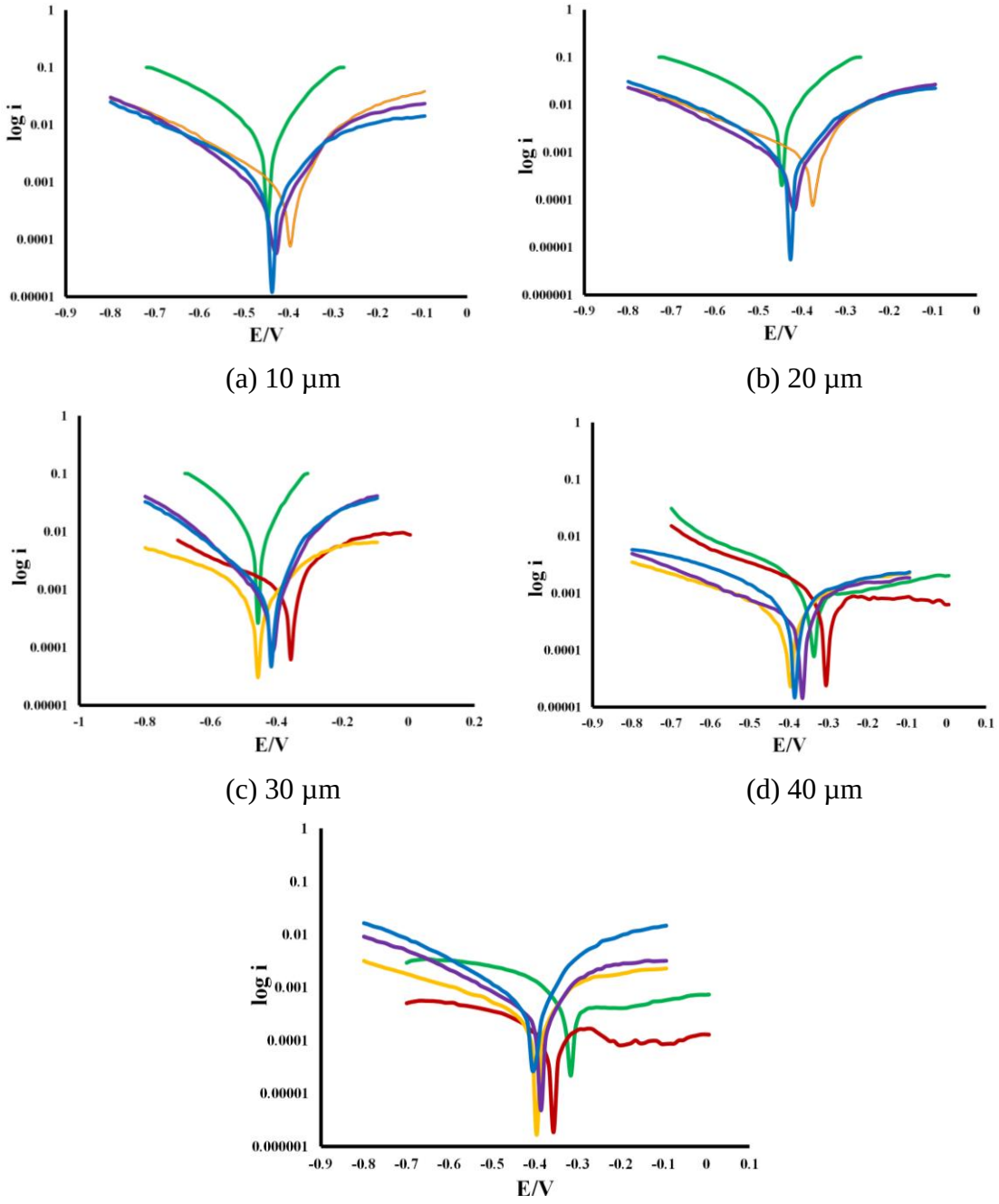

Figure 4.9 Scanning Tafel plots for PANI and PANI/MMT nanocomposites coated steel samples in 1M H_2SO_4 solution; (a) 10 µm, (b) 20 µm, (c) 30 µm, (d) 40 µm and (e) 50 µm; (——) PANI, (——) PANI/MMT 1 wt%, (——) PANI/MMT 3 wt%, (——) PANI/MMT 5 wt% and (——) PANI/MMT 7 wt%

Table 4.4 presents the corrosion potential (E_{corr}), corrosion current (I_{corr}), corrosion rate (CR) and % corrosion rate were calculated from Tafel plots of coated steel samples in 1M H_2SO_4. It can be seen that the corrosion rate and % CR of PANI/MMT nanocomposites coated samples were much lower than that of PANI coated samples. Therefore, the incorporation of MMT nanoparticles in PANI matrix promoted the anticorrosive efficiency of coated steel samples. From Table 4.4, for same thickness of PANI/MMT coated, corrosion rate decreased with increasing MMT loading. For same % MMT loading (1-7 wt%), the corrosion rate decreased with increasing thickness. Comparison of the corrosion rate of PANI/MMT nanocomposites coated on steel samples with various MMT loadings and thicknesses showed that the best anticorrosive properties of PANI/MMT nanocomposites coating with 5 wt% of MMT exhibited lowest corrosion rate for all coating thickness (10-50 µm) compared to 1, 3 and 7% MMT loading. The corrosion rate of PANI/MMT at 5 wt% of MMT coating was similar to the previous work reported by Ali Olad *et al*. [2]. The corrosion protection of PANI/MMT nanocomposites was enhanced compared to pure PANI coated samples. From the mechanism of corrosion protection, PANI coated samples induced the metal oxide formation on steel surface which shifted the corrosion potential of steel to the direction of noble steel and led to a decreasing in corrosion current [34]. In addition, silicate nanolayers of MMT dispersed in PANI matrix which increased the tortuosity of diffusion pathway of corrosive agents such as oxygen gas, hydrogen gas and hydroxide ions.

Therefore, % CR could be decreased by increase film thickness and MMT loading. For example, PANI/MMT at 5-7 wt% at 30 µm thickness (% CR = 12) and PANI/MMT at 1-3 wt% at 40 µm thickness (% CR = 7.4-11.8) have equivalent corrosion rate with PANI at 50 µm thickness (% CR = 10.4).

Figure 4.10 also shows that the % corrosion rate decreased with increasing % MMT loading (1-7 wt% MMT loading) and film thickness. Therefore, the corrosion protection of PANI/MMT nanocomposites is better than that of PANI coated samples.

Table 4.4 Corrosion potential (E_{corr}), corrosion current (I_{corr}), corrosion rate (CR) and % corrosion rate values calculated from Tafel plots for PANI and PANI/MMT at 1, 3, 5 and 7 %wt MMT content coated steel samples in 1M H_2SO_4 solution.

Sample	Thickness of layer (µm) ± 3 µm	E_{corr} (V)	I_{corr} (A/cm^2)	CR (mm/year)	% CR
Steel	-	-0.459	8.769×10^{-4}	10.17	100
PANI	10	-0.451	7.260×10^{-4}	8.418	82.8
PANI	20	-0.446	6.792×10^{-4}	7.875	77.4
PANI	30	-0.454	6.653×10^{-4}	7.713	75.8
PANI	40	-0.343	1.690×10^{-4}	1.950	19.2
PANI	50	-0.326	9.129×10^{-5}	1.058	10.4
PANI/MMT 1 wt%	10	-0.403	2.916×10^{-4}	3.380	33.2
PANI/MMT 1 wt%	20	-0.365	2.515×10^{-4}	2.916	28.7
PANI/MMT 1 wt%	30	-0.358	1.945×10^{-4}	2.254	22.2
PANI/MMT 1 wt%	40	-0.307	1.039×10^{-4}	1.204	11.8
PANI/MMT 1 wt%	50	-0.361	2.182×10^{-5}	0.253	2.5
PANI/MMT 3 wt%	10	-0.440	2.627×10^{-4}	3.064	30.1
PANI/MMT 3 wt%	20	-0.439	1.362×10^{-4}	1.580	15.5
PANI/MMT 3 wt%	30	-0.464	1.246×10^{-4}	1.445	14.2
PANI/MMT 3 wt%	40	-0.394	6.522×10^{-5}	0.756	7.4
PANI/MMT 3 wt%	50	-0.397	1.890×10^{-5}	0.219	2.2
PANI/MMT 5 wt%	10	-0.420	1.738×10^{-4}	2.015	19.8
PANI/MMT 5 wt%	20	-0.420	1.207×10^{-4}	1.399	13.8
PANI/MMT 5 wt%	30	-0.422	1.050×10^{-4}	1.217	12.0
PANI/MMT 5 wt%	40	-0.368	6.307×10^{-5}	0.731	7.2
PANI/MMT 5 wt%	50	-0.386	1.694×10^{-5}	0.197	1.9
PANI/MMT 7 wt%	10	-0.434	1.246×10^{-4}	1.445	14.2
PANI/MMT 7 wt%	20	-0.432	1.161×10^{-4}	1.346	13.2
PANI/MMT 7 wt%	30	-0.415	1.043×10^{-4}	1.209	11.9
PANI/MMT 7 wt%	40	-0.383	6.644×10^{-5}	0.770	7.6
PANI/MMT 7 wt%	50	-0.400	4.427×10^{-5}	0.513	5.0

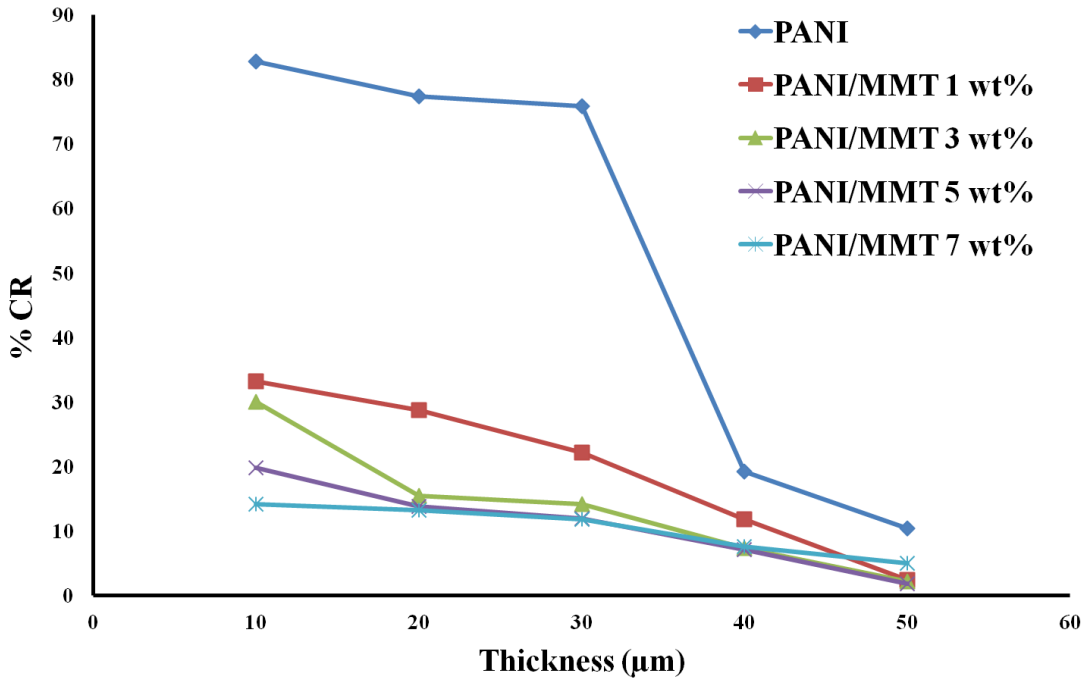

Figure 4.10 % Corrosion rate of PANI and PANI/MMT at 1, 3, 5 and 7 wt% MMT loading and 10-50 µm thickness

4.3.2 Morphology of PANI/MMT on Steel

The cross section morphology of coated steel sample with polymeric films of PANI or PANI/MMT nanocomposites before and after corrosion test was characterized by SEM; the magnification for 30 and 50 µm thickness of the nanocomposites were ×2000 and ×500, respectively. The morphology of the samples are shown in Figures 4.11-4.13.

For cross section morphology of the polymeric films of PANI/MMT nanocomposites before corrosion test, a good adherence was observed in the metal-polymer contact zone, regardless of the media used in the synthesis process. The cross section morphology of PANI/MMT (Figure 4.11) was similar to that reported by Rosa Vera *et al*. [25].

When comparing the polymeric films of PANI and PANI/MMT nanocomposites with 30 and 50 µm thickness after corrosion testing (Figures 4.12 and 4.13), the adhesion between PANI/MMT on steel 30 µm thickness was lower than that of 50 µm thickness because a pathway for diffusion of corrosive agent was short. However, the enhanced corrosion protection of PANI/MMT nanocomposites compared to PANI coated steel could be resulted from the dispersion of MMT layers in PANI matrix which increased the tortuosity of diffusion pathway of corrosion agents.

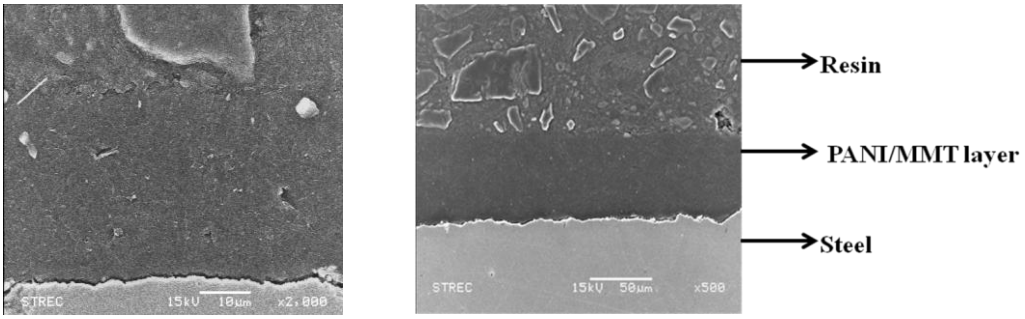

(a) (b)

Figure 4.11 Scanning electron micrographs of cross section of PANI/MMT at 3 wt% coating before corrosion test; (a) 30 µm (2,000x magnification) and (b) 50 µm (500x magnification).

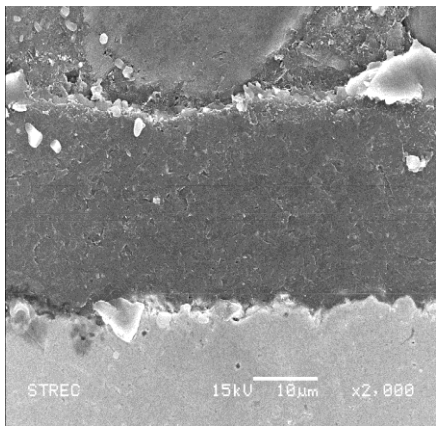

(a) PANI

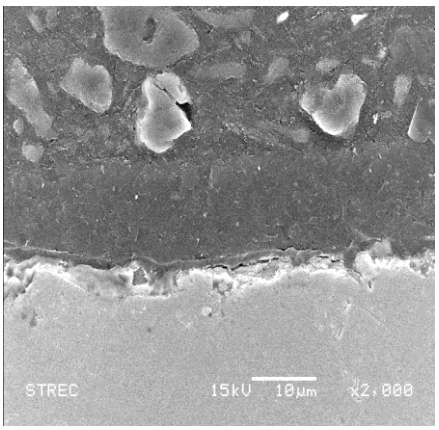

(b) PANI/MMT 1 wt%

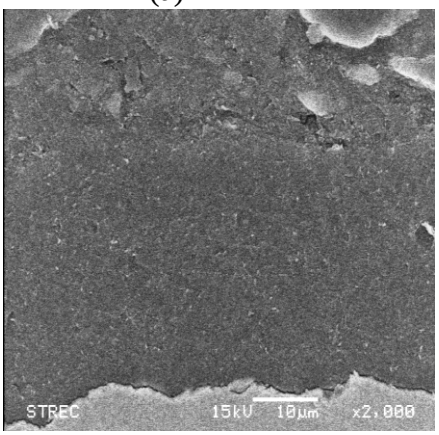

(c) PANI/MMT 3 wt%

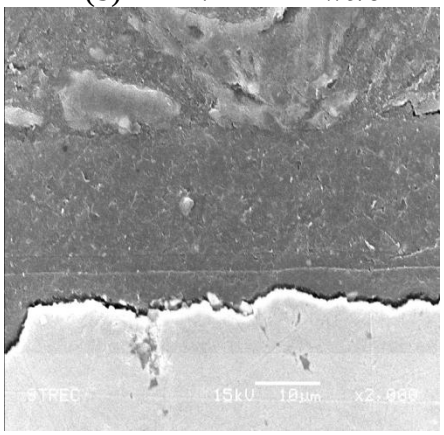

(d) PANI/MMT 5 wt%

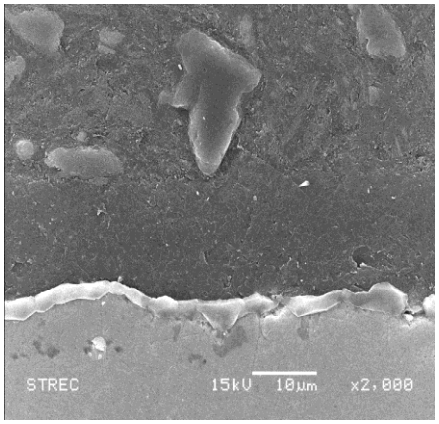

(e) PANI/MMT 7 wt%

Figure 4.12 Scanning electron micrographs of cross section of PANI and PANI/MMT nanocomposites coating (30 µm thickness) after corrosion test; (a) PANI, (b) PANI/MMT 1 wt%, (c) PANI/MMT 3 wt%, (d) PANI/MMT 5 wt% and (e) PANI/MMT 7 wt% (2,000x magnification).

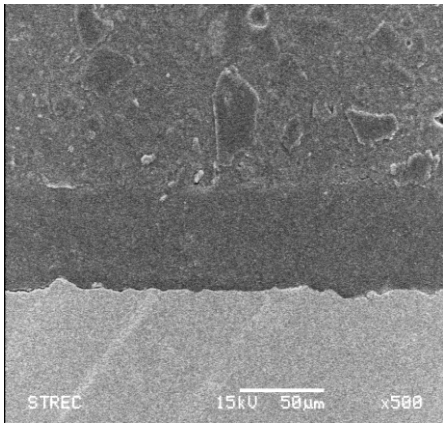

(a) PANI

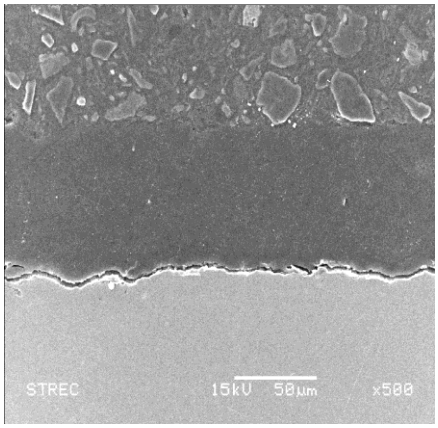

(b) PANI/MMT 1 wt%

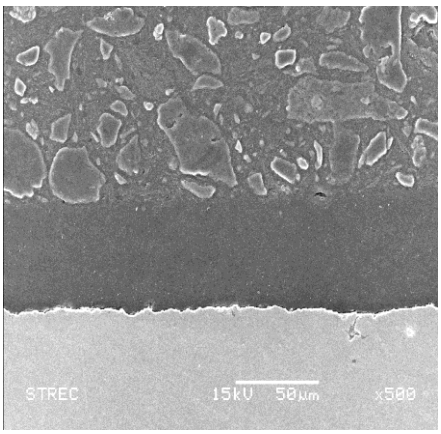

(c) PANI/MMT 3 wt%

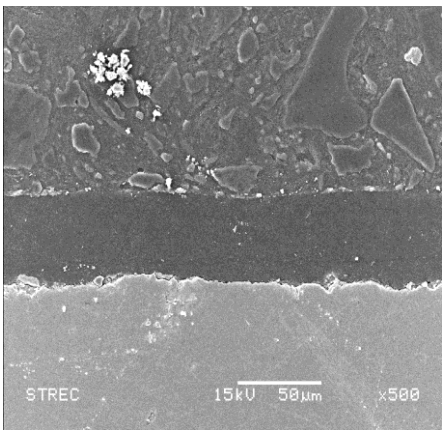

(d) PANI/MMT 5 wt%

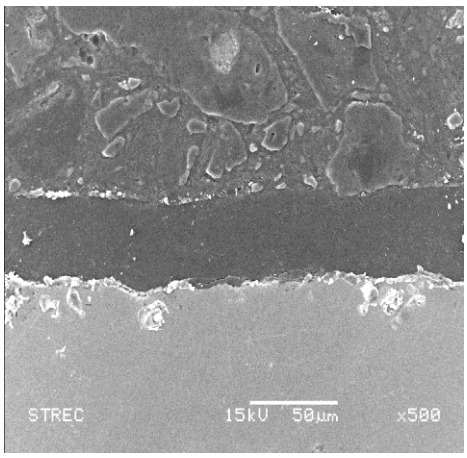

(e) PANI/MMT 7 wt%

Figure 4.13 Scanning electron micrographs of cross section of PANI and PANI/MMT nanocomposites coating (50 µm thickness) after corrosion test; (a) PANI, (b) PANI/MMT 1 wt% (c) PANI/MMT 3 wt%, (d) PANI/MMT 5 wt% and (e) PANI/MMT 7 wt% (500x magnification).

The surface morphologies of the polymeric films of PANI and PANI/MMT nanocomposites after corrosion test characterized by SEM are shown in Figures 4.14 and 4.15.

From Figures 4.14(a) and 4.15(a), the surface of the polymeric films of PANI with 30 and 50 μm thickness after corrosion test were rough and exhibited a cracking appearance indicated the deformation failure in corrosion test. Hence, the films of PANI had a lower corrosion resistance and inferior anticorrosive property. The corrosion mechanism of PANI is represented in Figure 4.16. The PANI coating showed cracking surface after the pollutant diffused through the film barrier and exposed to the steel surface. The corrosion products such as metal oxide was obtained under the cracking surface. For the addition of MMT into the PANI matrix, MMT filled aggregates within the PANI matrix. Therefore, the enhanced corrosion protection of PANI/MMT nanocomposites compared to PANI coated steel might result from the layers of MMT dispersed in PANI matrix which increased the tortuosity of diffusion pathway of corrosion agents [7]. The corrosion mechanism of PANI/MMT is represented in Figure 4.17. The diffusion of pollutants across the coating surface is the beginning of corrosion process. The electrochemical corrosion reaction was occured at poor adherence area and the corrosion products were obtained below the swelling surface. The addition of MMT showed an improvement of anticorrosion properties where 5 wt% of MMT loading with 50 μm film thickness exhibited the best compatibility (Figure 4.15(d)). The surface morphologies of PANI/MMT (Figure 4.14) was similar to that reported polyaniline (PANI) and poly-ortho-methoxyaniline (POMA) by Rosa Vera *et al*. [25].

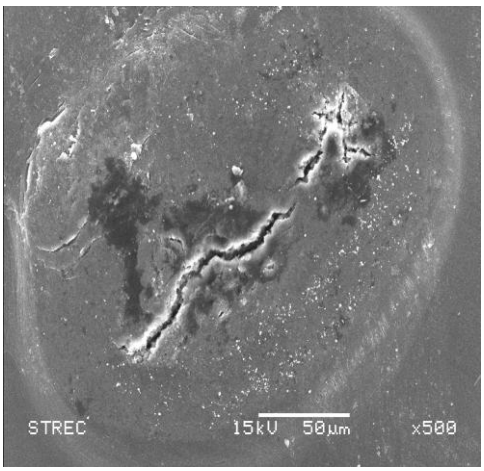

(a) PANI

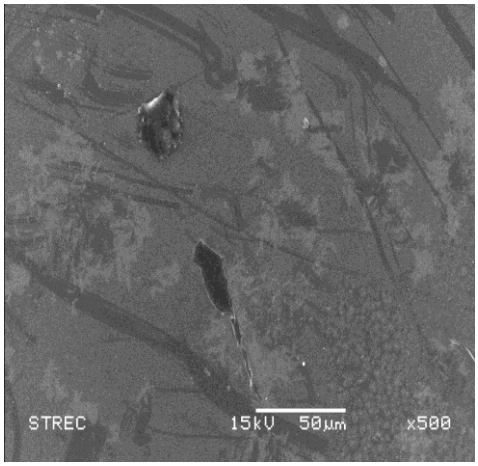

(b) PANI/MMT 1 wt%

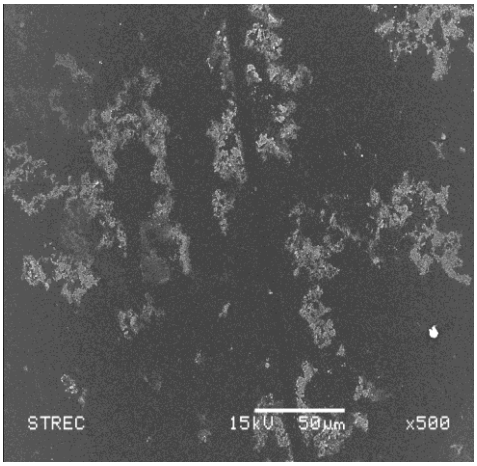

(c) PANI/MMT 3 wt%

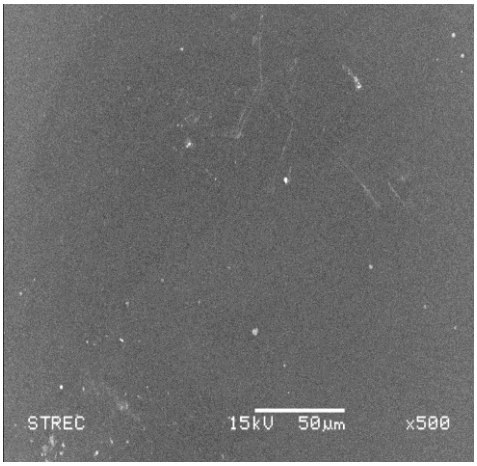

(d) PANI/MMT 5 wt%

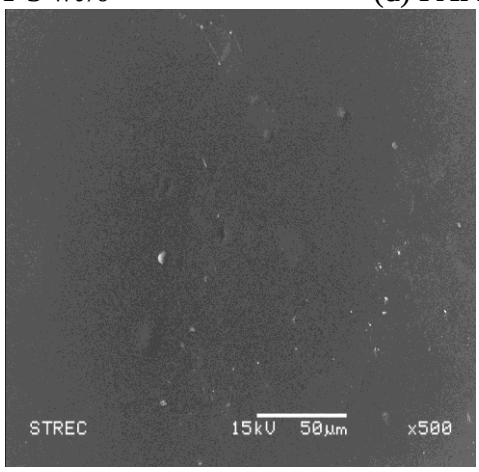

(e) PANI/MMT 7 wt%

Figure 4.14 Scanning electron micrographs of surface area of PANI and PANI/MMT nanocomposites coating (30 µm thickness) after corrosion test; (a) PANI, (b) PANI/MMT 1 wt% (c) PANI/MMT 3 wt%, (d) PANI/MMT 5 wt% and (e) PANI/MMT 7 wt% (500x magnification).

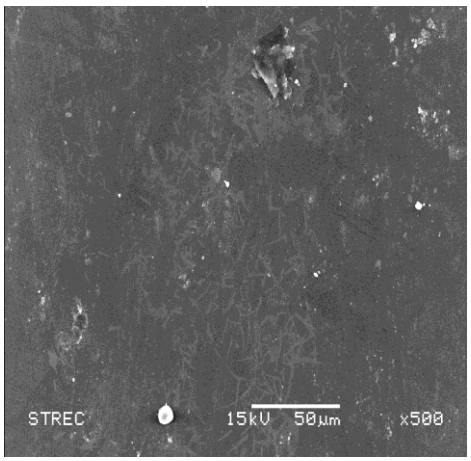

(a) PANI

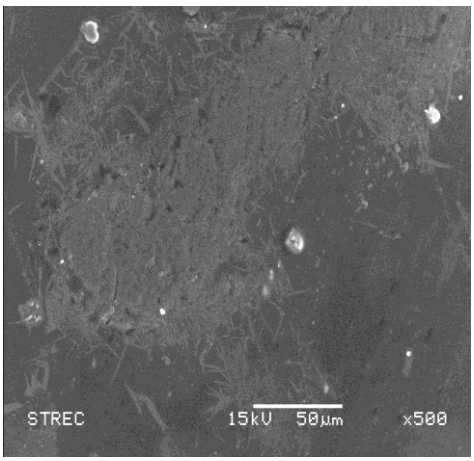

(b) PANI/MMT 1 wt%

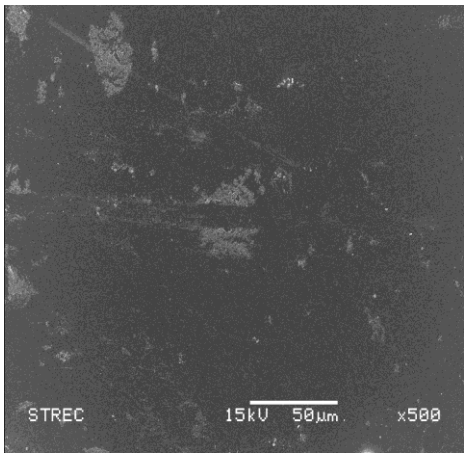

(c) PANI/MMT 3 wt%

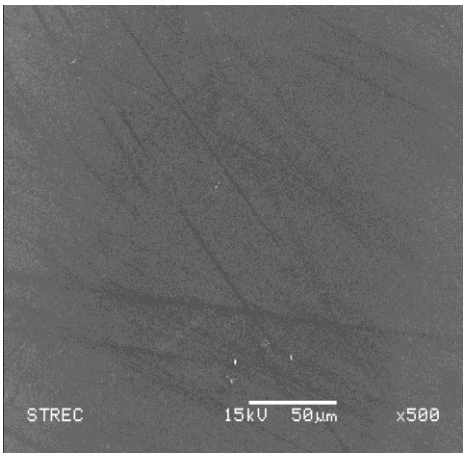

(d) PANI/MMT 5 wt%

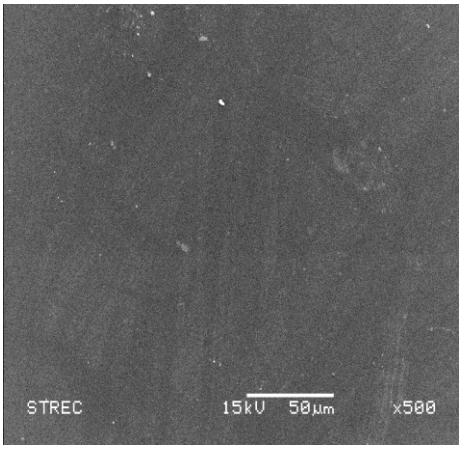

(e) PANI/MMT 7 wt%

Figure 4.15 Scanning electron micrographs of surface area of PANI and PANI/MMT nanocomposites coating (50 µm thickness) after corrosion test; (a) PANI, (b) PANI/MMT 1 wt% (c) PANI/MMT 3 wt%, (d) PANI/MMT 5 wt% and (e) PANI/MMT 7 wt% (500x magnification).

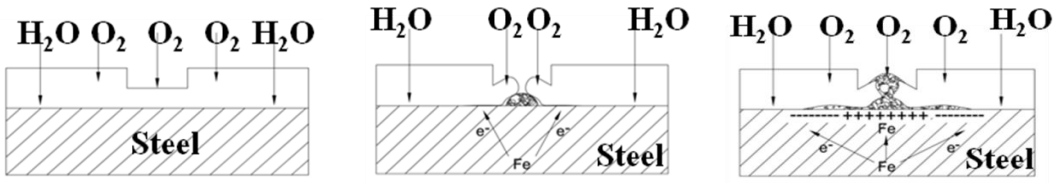

(a) (b) (c)

Figure 4.16 Corrosion mechanism of PANI coatings; (a) initial state of the surface, (b) pollutants access and pollutants diffusion and (c) corrosion products obtained under the surface

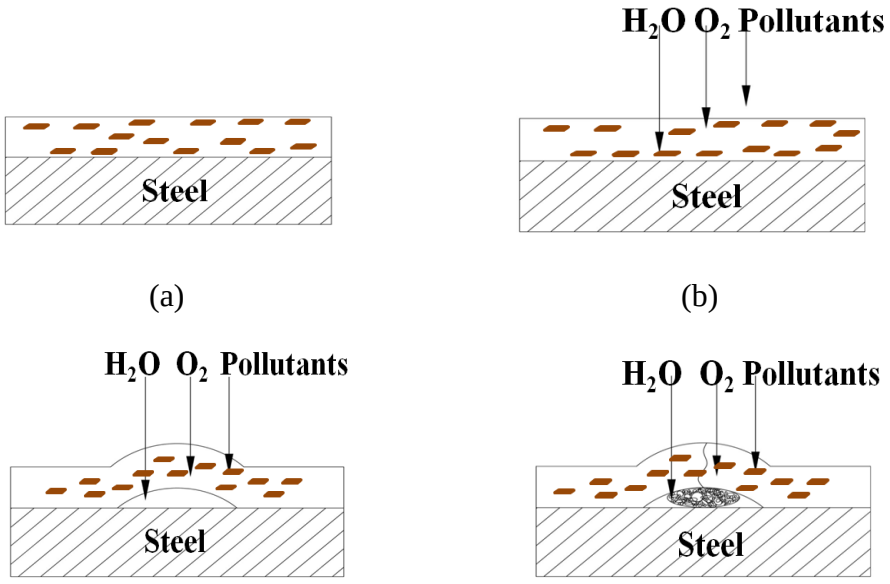

(a) (b)

(c) (d)

Figure 4.17 Corrosion mechanism of PANI/MMT coatings; (a) initial state of the surface, (b) pollutants access, (c) pollutants diffusion and layer swelling and (c) corrosion products obtained under the surface

4.3.3 Salt Spray Test

Figure 4.18 illustrated the coupons of coated steel with PANI and PANI/MMT at 1-5 wt% (30 µm and 50 µm thickness) after the salt spray test for 97 hours. The film of PANI at 30 µm and 50 µm thickness (Figure 4.18(a)-(b)) showed the surface flawed and cracked at the cut edge of the sample at 48 h, leading to very rapid rusting. From Figure 4.18 (c)-(h), the coated samples with PANI/MMT at 1-5 wt% at 30 µm and 50 µm thickness had no rust. The coating system was able to protect the steel substrate in accelerated corrosion test. The results showed PANI coatings did not improve corrosion protection significantly as evaluated by salt spray test. However, for PANI/MMT nanocomposites coating, the corrosion protection increased significantly. The PANI/MMT nanocomposites coating could withstand over 97 hours of salt spray without flawed and cracked on the specimen. Therefore, the corrosion protection of PANI/MMT nanocomposites coating is better than that of PANI coated samples at 30 µm and 50 µm thickness.

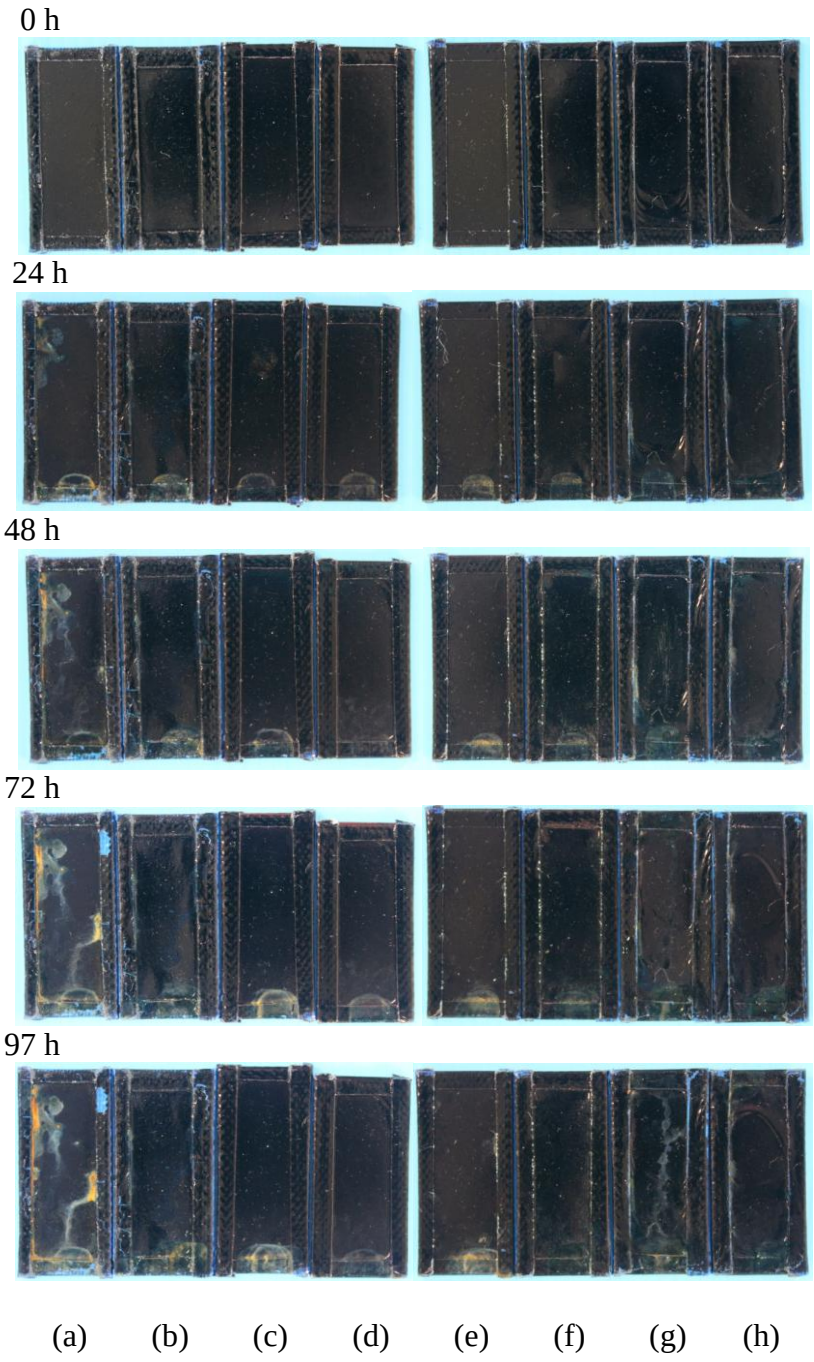

Figure 4.18 Coupons of coated steel of PANI and PANI/MMT nanocomposites coating after salt spray test for 0, 24, 48 72 and 97 h; (a) PANI at 30 µm thickness, (b) PANI at 50 µm thickness, (c) PANI/MMT 1 wt% at 30 µm thickness, (d) PANI/MMT 1 wt% at 50 µm thickness, (e) PANI/MMT 3 wt% at 30 µm thickness, (f) PANI/MMT 3 wt% at 50 µm thickness, (g) PANI/MMT 5 wt% at 30 µm thickness and (h) PANI/MMT 5 wt% at 30 µm thickness.

CHAPTER V

CONCLUSIONS AND SUGGESTIONS

5.1 Conclusions

PANI/MMT nanocomposites were successfully synthesized by *in situ* chemical oxidative polymerization. The high monomer conversion of 75.8% was achieved at 1 wt% MMT loading. For PANI/MMT nanocomposites, the insertion of a polymer chain into the layered silicate structure occurs in a crystallographically regular fashion, regardless of the clay to polymer ratio. Intercalated nanocomposites are normally interlayer by a few molecular layers of polymer, as confirmed by X-ray diffractometer.

SEM micrograph of PANI/MMT nanocomposites showed the MMT layer and the agglomerated spheres of PANI dispersion on the nanocomposites surface. From thermogravimetric analysis, the thermal stability of the PANI/MMT nanocomposites increased with an increasing in the amount of MMT, and the maximum degradation temperature of 568°C was achieved resulting in an excellent thermal stability.

The corrosion rates of PANI/MMT nanocomposites were lower than that of PANI coated. The steel coated with 50 μm thickness of PANI/MMT (5 wt%) showed the best corrosion resistance comparing to the other coating. From SEM micrograph, the surface cracking of polymeric films of PANI/MMT nanocomposites was lower than that of PANI. Therefore, the corrosion protection of PANI/MMT nanocomposites was enhanced comparing to PANI coated on steel. The enhancement of corrosion protection of PANI/MMT nanocomposites compared to PANI coated samples might be resulted from metal oxide formation on the steel surface induced by PANI coated and silicate nanolayers of MMT dispersed in PANI matrix which increased the tortuosity of diffusion pathway of corrosive agents such as oxygen gas, hydrogen gas and hydroxide ions.

From salt spray test, the corrosion protection increased significantly. The PANI/MMT nanocomposites coatings could withstand over 97 hours of salt spray.

Therefore, the corrosion protection of PANI/MMT nanocomposites coatings is better than that of PANI coated samples at 30 μm and 50 μm thickness.

5.2 Suggestions of the Future Work

A future investigation of PANI/MMT nanocomposites should be carried out with the following aspects:

1. Synthesis of PANI/MMT nanocomposites
   The effect of molecular weight, viscosity, dispersion of MMT in PANI matrix on the preparation of PANI/MMT nanocomposites should be further studied.
2. Synthesis of PANI/zeolite nanocomposites
   The synthesis of PANI/zeolite nanocomposites should be further studied by using zeolite for providing the good corrosion protection due to the ability to promote the barrier property of PANI against aggressive species.
3. Synthesis of PANI/MMT containing vinyl coating
   The PANI/MMT containing vinyl coating should be further studied for improving the corrosion protection.
4. Application of PANI/MMT nanocomposites
   The preparation of PANI/MMT nanocomposites should be further studied for improving the mechanical properties. In addition, gas barrier properties (permeability of film) should be explored.

REFERENCES

[1] Pierre, R. Roberge. Corrosion Engineering: Principles and Practice. United States of America: Mc Graw-Hill, 2008.

[2] Olad, A. Naseri, B. Preparation, characterization and anticorrosive properties of novel polyaniline/clinoptilolite nanocomposite. *Progress in Organic Coatings* 67 (2010): 233–238.

[3] Gonzalez, M. Soares, B.G. Magioli, M. Marins, J.A. and Rieumont, J. Facile method for synthesis of polyaniline/silica hybrid composites by simultaneous sol-gel process and "in situ" polymerization of aniline. *Journal of Sol-Gel Science Technology* 63 (2012): 373–381.

[4] Yeh, J.-M. and Chang, K. C. Polymer/layered silicate nanocomposite anticorrosive coatings. *Journal of Industrial and Engineering Chemistry* 14 (2008): 275-291.

[5] Pinnavaia, T.J. and Beall, G.W. Polymer-Clay Nanocomposites. 2000, John Wiley & Sons: West Sussex, England. p. 97-109.

[6] Bhadra, S. Khastgir, D. Singha, N.K. and Lee, J.H. Progress in preparation, processing and applications of polyaniline. *Progress in Polymer Science* 34 (2009): 738-810.

[7] Olad, A. and Rashidzadeh, A. Preparation and anticorrosive properties of PANI/Na-MMT and PANI/O-MMT nanocomposites. *Progress in Organic Coatings* 62 (2008): 293-298.

[8] Skotheim, T.A. and Reynolds, J.R. Conjugated Polymers: Processing and Applications. 3rd ed., New York: Taylor & Francis Group, 2007.

[9] Nalwa, H.S. Conductive Polymers: Synthesis and Electrical Properties. 1997, John Wiley & Sons: West Sussex, England. p. 506-517.

[10] Deer, W.A., Howie, R.A. and Zussman, J. An Introduction to the Rock-forming minerals. China: Addition Wesley Longmann, 1996.

[11] Zeng, Q.H. Yu, A.B. Lu, G.Q. and Paul, D.R. Clay-based polymer nanocomposites: research and commercial development. *Journal of Nanoscience and Nanotechnology* 5 (2005):1574–92.

[12] Mai, Y.-W. and Yu, Z.-Z. Polymer Nanocomposites. 2000, Woodhead Publishing: Cambridge, England. p. 59-62.

[13] Bosich, J.F. Corrosion Prevention for Practicing Engineers. 1970, Barnes & Noble, Inc: New York, US. p. 1-15.

[14] *Galvanic Corrosion*. [online]. 2013. Available from: http://octane.nmt.edu/Water Quality/corrosion/Galvanic.aspx [2013, March 9]

[15] *Crevice or Concentration cell Corrosion, and Exception to Pitting Corrosion*. [online]. 2013. Available from: http://www.clihouston.com/knowledge-base/crevice-or-concentration-cell-corrosion-and-exception-to-pitting-corrosion.html [2013, March 9]

[16] *Pitting Corrosion*. [online]. 2013. Available from: http://www.materialsengineer.com/ G-Pitting-Corrosion.htm [2013, March 9]

[17] *Stress Corrosion Cracking*. [online]. 2013. Available from: http://www.cdcorrosion.com/mode_corrosion/stress_corrosion_cracking.htm [2013, March 9]

[18] *Intergranular Corrosion*. [online]. 2013. Available from: http://www.cdcorrosion.com/mode_corrosion/corrosion_intergranular.htm [2013, March 9]

[19] *Corrosion in Material of Construction*. [online]. 2013. Available from: http://majarimagazine.com/2009/01/corrosion-in-material-of-construction/ [2013, March 9]

[20] Laco, J.I.I. Villota, F.C. and Mestres, F.L. Corrosion protection of carbon steel with thermoplastic coatings and alkyd resins containing polyaniline as conductive polymer. *Progress in Organic Coatings* 52 (2005): 151-160.

[21] Narayanan, B.N. Koodathil, R. Gangadharan, T. Yaakob, Z. Saidu, F.K. and Chandralayam, S. Preparation and characterization of exfoliated polyaniline/montmorillonite nanocomposites. *Materials Science and Engineering B* 168 (2010): 242-244.

[22] Soundararajah, Q.Y. Karunaratne, B.S.B. and Rajapakse, R.M.G. Montmorillonite polyaniline nanocomposites: Preparation, characterization and investigation of mechanical properties. *Materials Chemistry and Physics* 113 (2009): 850-855.

[23] Bober, P. Stejskal, J. Spirkova, M. Trchova, M. Varga, M. and Prokes, J. Conducting polyaniline-montmorillonite composites. *Synthetic Metals* 160 (2010): 2596-2604.

[24] Ebrahimi, M. Akbarinezhad, E. and Sharif, F. Synthesis of exfoliated polyaniline-clay nanocomposite in supercritical CO_2. *The Journal of Supercritical Fluids* 59 (2011): 124-130.

[25] Vera, R. Romero, H. and Ahumada, E. Synthesis and characterization of polyaniline and poly-ortho-methoxyaniline. Behaviour against carbon steel corrosion. *Journal of the Chilean Chemical Society*. (2003) doi: 10.4067/S0717-97072003000100007.

[26] Kamaraj, K. Sathiyanarayanan, S. Muthukrishnan, and Venkatachari, G. Corrosion protection of iron by benzoate doped polyaniline containing coatings. *Progress in Organic Coatings* 64 (2009): 460-465.

[27] Venkatachari, G. Sathiyanarayanan, S. and Muthkrishnan, S. Corrosion protection of steel by polyaniline blended coating. *Electrochimica Acta* 51 (2006): 6313-6319.

[28] Radhakrishnan, S. Siju, C.R. Mahanta, D. Patil, s. and Madras, G. Conducting polyaniline-nano-TiO_2 composites for smart corrosion resistant coatings. *Electrochimica Acta* 54 (2009): 1249-1254.

[29] Liu, Y.D. Fang, F.F. Choi, H.J. and Seo, Y. Fabrication of semiconducting polyaniline/nano-silica nanocomposite particles and their enhanced electrorheological and dielextric characteristics *Colloids and Surfaces A: Physicochemical and Engineering Aspects* 381 (2011): 17-22.

[30] Narayanan, B.N. Koodathil, R. Gangadharan, T. Yaakob, Z. Saidu, F.K. and Chandralayam, S. Preparation and characterization of exfoliated polyaniline/montmorillonite nanocomposites. *Materials Science and Engineering B* 168 (2010): 242-244.

[31] Narayanan, B.N. Koodathil, R. Gangadharan, T. Yaakob, Z. Saidu, F.K. and Chandralayam, S. Preparation and characterization of exfoliated polyaniline/montmorillonite nanocomposites. *Materials Science and Engineering B* 168 (2010): 242-244.

[32] *Product bulletin*. [online]. 2013. Available from: http://www.scprod.com/product_bulletins/PB%20Cloisite%2015.pdf [2013, May 7]

[33] Vilela, S.O. Soto-Oviedo, M.A. Albers, A.P.F. and Faez, R. Polyaniline and Mineral Clay-based Conductive Composites. *Materials Research* 10 (2007): 297-300.

[34] Martyak, N.M. and McAndrew, P. Corrosion performance of steel coated with co-polyamides and polyaniline. *Corrosion Science* 49 (2007): 3826-3837.

APPENDICES

Appendix A

The Properties of Montmorillonite and Chemical Composition of the Steel Samples

Table A-1 Properties of montmorillonite clay (Cloisite15A)

Properties	Cloisite15A
Organic Modifier	2M2HT
Modifier Concentration	125 meq/100 g clay
% Moisture	< 2%
% Weight loss on ignition	43%
Specific Gravity	1.66
Color	Off white
Typical Dry Particle Sizes (microns, by volume)	10% less than 2 µ 50% less than 6 µ 90% less than 13 µ
Initial *d*-spacing	3.15 nm

All results from product bulletin of Southern Clay Product

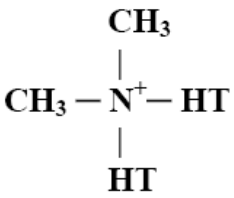

Where HT is Hydrogenated Tallow (~65% C18; ~30% C16; ~5% C14)
Anion: Chloride
2M2HT: dimethyl, dehydrogenated tallow, quaternary ammonium

Table A-2 Chemical composition of the steel spring sheet (SK5)

Element	**Percent (w/w, %)**
Fe	99.71
Mn	0.25
Cr	0.04

Appendix B

Calculation of Monomer Conversion

$$Monomer\,Conversion(\%) = \frac{M_0 - M_1}{M_2} x100 \qquad \text{(B.1)}$$

where; M_0 = Mass of the resulting composite particles (gram)

M_1 = Mass of the charged MMT particles (gram)

M_2 = Mass of the charged aniline monomer (gram)

Table B.1 Monomer conversion calculation and standard seviation

Experiment	MMT loading (%)	M_0 (g)	M_1 (g)	M_2 (g)	%Monomer Conversion
PANI	0	3.1512	0	4.0868	77.11
PANI	0	3.0595	0	4.0868	74.86
PANI	0	3.1655	0	4.0868	77.46
PANI	0	3.1833	0	4.0868	77.89
Mean					78.50
SD					1.35
PANI/MMT 1 wt%	1	3.2728	0.041	4.0868	79.08
PANI/MMT 1 wt%	1	3.2695	0.041	4.0868	77.00
PANI/MMT 1 wt%	1	2.9226	0.041	4.0868	70.51
PANI/MMT 1 wt%	1	3.0909	0.041	4.0868	74.63
Mean					75.81
SD					3.68
PANI/MMT 3 wt%	3	3.3326	0.123	4.0868	78.54
PANI/MMT 3 wt%	3	3.1826	0.123	4.0868	74.87
PANI/MMT 3 wt%	3	3.0203	0.123	4.0868	70.89
PANI/MMT 3 wt%	3	3.0518	0.123	4.0868	71.66
Mean					73.99
SD					3.49
PANI/MMT 5 wt%	5	3.2916	0.204	4.0868	75.55
PANI/MMT 5 wt%	5	3.3708	0.204	4.0868	77.49
PANI/MMT 5 wt%	5	3.0462	0.204	4.0868	69.55
PANI/MMT 5 wt%	5	3.0933	0.204	4.0868	70.70
Mean					73.32
SD					3.81
PANI/MMT 7 wt%	7	3.2388	0.286	4.0868	72.25
PANI/MMT 7 wt%	7	3.2389	0.286	4.0868	72.25
PANI/MMT 7 wt%	7	3.3729	0.286	4.0868	75.53
PANI/MMT 7 wt%	7	3.2856	0.286	4.0868	73.40
Mean					73.36
SD					1.55

Appendix C

Appearance of PANI/MMT nanocomposites

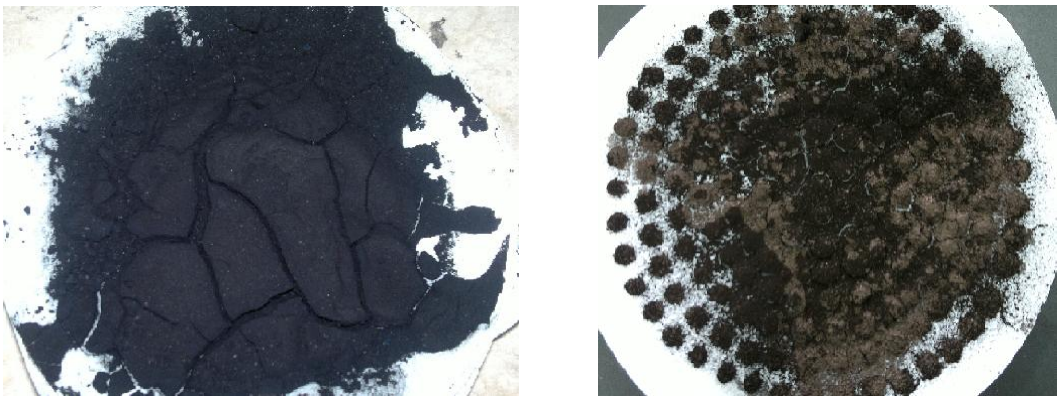

(a) (b)

Figure C.1 Appearance of (a) PANI/MMT EMERALDINE SALT (green) and (b) PANI/MMT EMERALDINE BASE (brown)

Appendix D

Chemical Composition of the Steel Samples

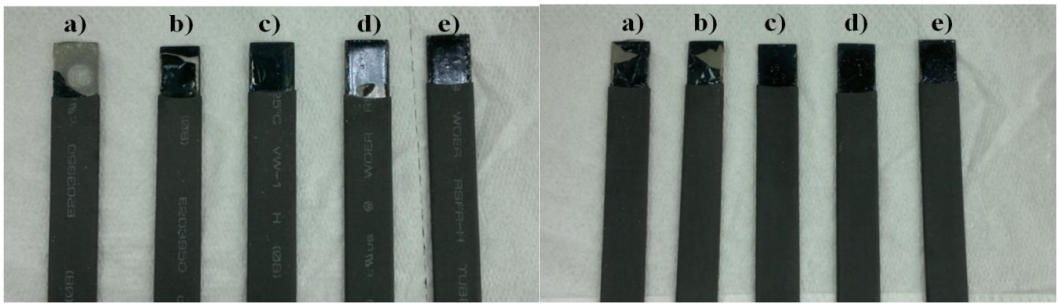

(a) (b)

Figure D.1 Appearance of coupons of coated steel with PANI at 10 µm to 50 µm thickness (a)-(e)) after the electrochemical Tafel slope analysis; (a) front and (b) back

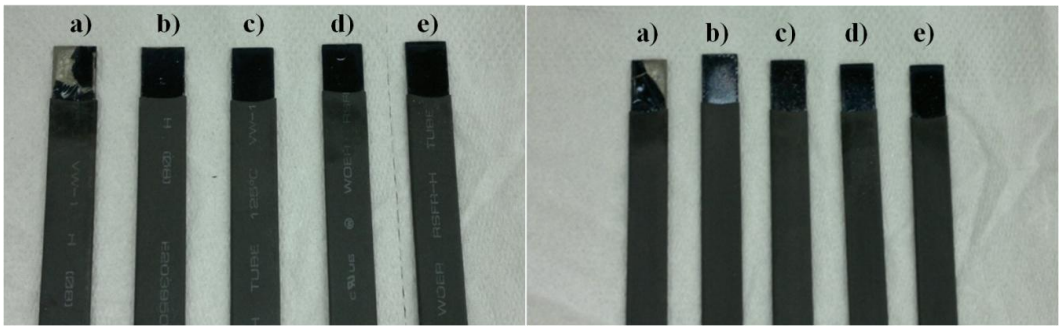

(a) (b)

Figure D.2 Appearance of coupons of coated steel with PANI/MMT at 1 wt% at 10 µm to 50 µm thickness (a)-(e)) after the electrochemical Tafel slope analysis; (a) front and (b) back

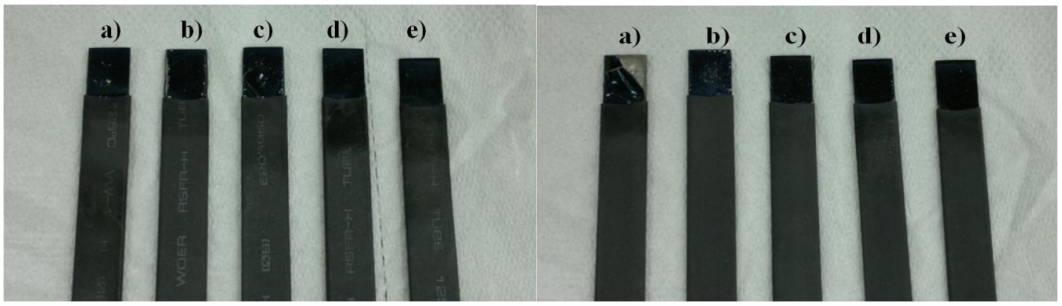

(a) (b)

Figure D.3 Appearance of coupons of coated steel with PANI/MMT at 3 wt% at 10 µm to 50 µm thickness (a)-(e)) after the electrochemical Tafel slope analysis; (a) front and (b) back

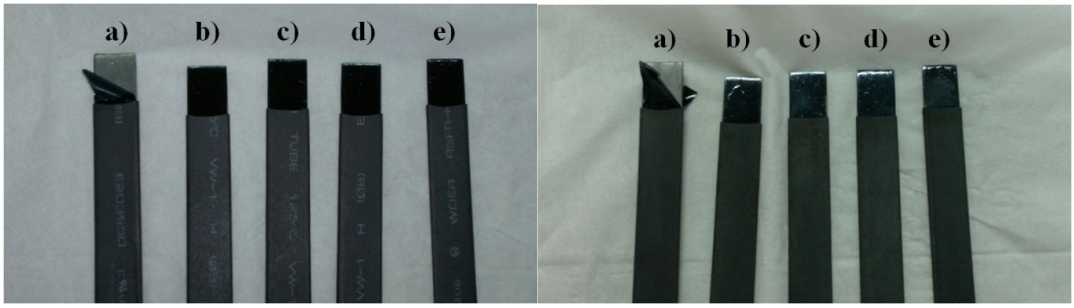

(a) (b)

Figure D.4 Appearance of coupons of coated steel with PANI/MMT at 5 wt% at 10 µm to 50 µm thickness (a)-(e)) after the electrochemical Tafel slope analysis; (a) front and (b) back

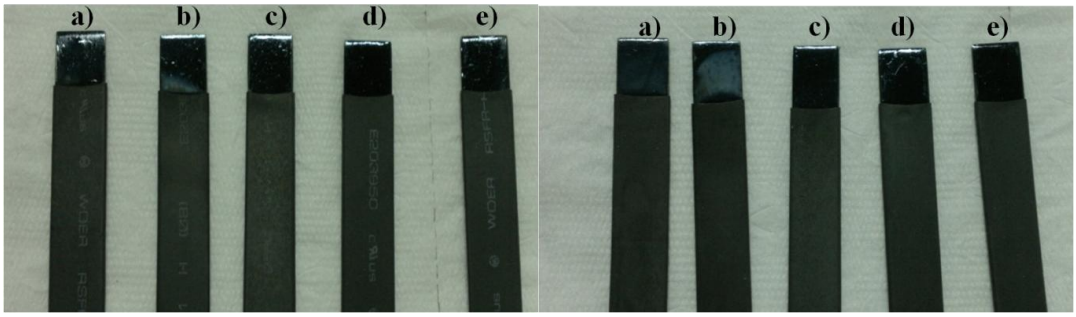

(a) (b)

Figure D.5 Appearance of coupons of coated steel with PANI/MMT at 7 wt% at 10 µm to 50 µm thickness (a)-(e)) after the electrochemical Tafel slope analysis; (a) front and (b) back

VITA

Miss Pattama Pironruen was born on September 18, 1987 in Saraburi, Thailand. She received her Bachelor's degree of Industrial Chemistry, King Mongkut's Institute of Technology Ladkrabang. She was admitted to Master Degree in the Program of Petrochemistry and Polymer Science, Chulalongkorn University as student in 2010 and finished her study in 2013.

Presentations at the National Conference

"Polyaniline/Montmorillonite Nanocomposites for Corrosion Protection of Steel", January 23-25, 2013. Pure and Applied Chemistry International Conference 2013 (PACCON 2013), Chonburi, Thailand.